Chemical Science

ROYAL SOCIETY OF CHEMISTRY

PERSPECTIVE

View Article Online
View Journal | View Issue

Cite this: *Chem. Sci.*, 2023, **14**, 1641

All publication charges for this article have been paid for by the Royal Society of Chemistry

Received 7th August 2022
Accepted 11th December 2022

DOI: 10.1039/d2sc04397a

rsc.li/chemical-science

Synchrotron radiation based *operando* characterization of battery materials

Ashley P. Black, [a] Andrea Sorrentino, [b] François Fauth, [b] Ibraheem Yousef, [b] Laura Simonelli, [b] Carlos Frontera, [a] Alexandre Ponrouch, [a] Dino Tonti [a] and M. Rosa Palacín *[a]

Synchrotron radiation based techniques are powerful tools for battery research and allow probing a wide range of length scales, with different depth sensitivities and spatial/temporal resolutions. *Operando* experiments enable characterization during functioning of the cell and are thus a precious tool to elucidate the reaction mechanisms taking place. In this perspective, the current state of the art for the most relevant techniques (scattering, spectroscopy, and imaging) is discussed together with the bottlenecks to address, either specific for application in the battery field or more generic. The former includes the improvement of cell designs, multi-modal characterization and development of protocols for automated or at least semi-automated data analysis to quickly process the huge amount of data resulting from *operando* experiments. Given the recent evolution in these areas, accelerated progress is expected in the years to come, which should in turn foster battery performance improvements.

Introduction

World transition towards a less fossil fuel dependent energy economy can be achieved by widespread deployment of energy storage technologies at large (grid) and intermediate (vehicle) scales. In view of their efficiency and versatility, rechargeable batteries are currently being considered for such applications, which face a different set of technical requirements (*e.g.* in terms of cost and lifetime), when compared to their use in portable electronics.

Research efforts are thus on course worldwide to improve currently available battery chemistries, such as Li-ion, while at the same time looking for new concepts with high energy density and/or advantages in terms of cost and sustainability.

Batteries being intrinsically complex devices,[1] mastering materials science in general, and characterization techniques in particular, is crucial to achieve progress in both research directions.

Measurements done *in situ* (inside the battery) or *operando* (taken during cell functioning) have lately boosted and improved in spectral/spatial resolution for a myriad of techniques, including diffraction and a wide spectrum of spectroscopic and imaging techniques (and even combinations thereof). Different length scales need to be probed: from Å to nm for surfaces/interfaces, and from tens of nm to μm for electrode materials, to reach mm for full electrodes and full devices.[2,3] Moreover, due attention has to be paid to the sensitivity of the technique (surface *vs.* bulk) and to time resolution, which will determine the feasibility of mapping in dynamic processes. Beyond the use of standard state-of-the-art laboratory equipment, synchrotron radiation stands out as one of the most powerful tools within battery research.[4] It allows non-destructive probing of materials with various depth sensitivities allowing fast acquisition rates, large penetration depths, high spectral or spatial resolution, and access to techniques that are only possible with a continuous tuneable source over a wide photon energy range. The use of *operando* techniques has intrinsic advantages, as they enable the detection of possible metastable intermediates and ensure characterization under real conditions (non-equilibrium) avoiding the risk of *ex situ* sample evolution during manipulation. *Operando* experiments are thus crucial for both the elucidation of redox mechanisms in new technologies and also understanding of failure and ageing processes for already commercial concepts, and thus their use is becoming widespread. However, compatibility between the electrochemical cell architectures and the experimental set-ups may force some specific design features and care has to be taken to ensure that these do not perturb the electrochemical response of the materials under investigation.[5]

Synchrotron radiation involves a wide range of photon energies. X-rays with energies above ~4 keV are called "hard" X-rays, while those with much lower energies (and longer wavelengths) are called "soft" X-rays. The former have a larger penetration (lower absorption cross section) probing depths from a few μm to the mm range, while the latter exhibit much higher cross sections and penetration below a few μm of

[a]*Institut de Ciència de Materials de Barcelona, ICMAB-CSIC, Campus UAB, 08193 Bellaterra, Catalonia, Spain. E-mail: rosa.palacin@icmab.es*

[b]*CELLS – ALBA Synchrotron, 08290 Cerdanyola del Vallès, Catalonia, Spain*

probing depths, being therefore much more surface sensitive. "Tender" X-rays (TX) represent an intermediate region with energies between 1 and 4 keV.

This perspective focuses on the state-of-the art of *operando* techniques using synchrotron radiation applied to batteries, covering from hard to soft X-rays. The first section describes the requirements for the experimental set-up, with emphasis on techniques where broader experience exists. They have been classified into three broad groups, which reflect differences in the type of radiation/matter interactions and also data analysis approaches and requirements. The second section covers techniques that are based on elastic (kinetic energy conserved) scattering, including not only diffraction (probing long range ordering) but also SAXS (Small Angle X-ray Scattering) and PDF (Pair Distribution Function), the latter providing inputs at a local scale. The third section deals with absorption or emission based spectroscopic techniques, which access the electronic structure and enable additional chemical insights: XAS (X-ray Absorption Spectroscopy) which has been well developed to perform *operando* experiments using hard, soft and tender X-rays and also other techniques which in this sense are less mature to date such as XPS (X-ray Photoelectron Spectroscopy) or infrared spectroscopy. The fourth section is devoted in general to imaging techniques and tomography, which, despite intrinsic physical differences, typically generate the largest datasets. Last but not least, a final Discussion and Outlook section provides the authors' view on the evolution of the field and the workarounds that may be developed in the next few years.

Electrochemical cell & setup requirements

Besides generic electrochemical cell requirements (corrosion resistance, good electric contact, tightness to avoid liquid electrolyte leakage or exposure to air of any sensitive samples), the setups used for *operando* X-ray scattering measurements need to be compatible with prolonged exposure to the beam, having the lowest possible absorption, although the latter is much less critical when using synchrotron radiation. A relevant factor is the photon energy, which largely affects the penetration depth (see Fig. 1), and eventual vacuum requirements. In general, for all the experiments which require transmission, the electrochemical cell has to be designed to be as X-ray transparent as possible optimizing the choice of materials and component thickness.

Rigid material windows ensure stack pressure and hence good electric contact. This is an often overlooked aspect, but uniform pressure is also critical for reliable electrochemical data, especially over extended cycling periods. Beryllium is the most transparent metal and widely used window, its drawbacks being high cost, toxicity and lack of stability at high potentials (becoming itself oxidized), the latter being usually alleviated by the use of an additional foil (*e.g.* aluminium). Yet, other thin metal foils are also an option,[7] provided that absorption is not too high, or even insulating materials (glass), that can also be

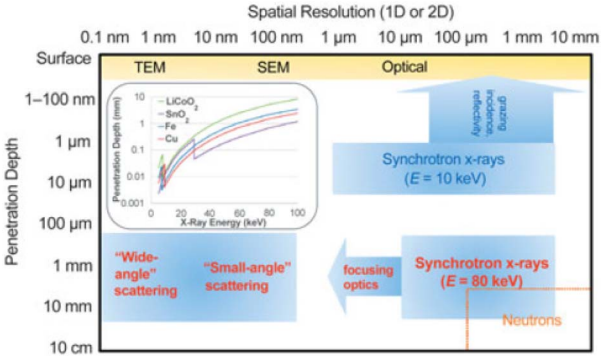

Fig. 1 Typical penetration depth and spatial resolution (1D and 2D measurements) for selected analytical techniques. The inset depicts 1/*e* penetration depths for various battery relevant materials as a function of energy (*E*), where *e* is Euler's number. TEM and SEM stand for Transmission Electron Microscope and Scanning Electron Microscope, respectively. Reproduced from ref. 6 with permission, © Materials Research Society.

covered by a metal foil to enhance electronic conductivity. Note that when the same cell setup is to be employed for scattering and XAS (X-ray Absorption Spectroscopy) experiments, thin Kapton (polyimide) is used to minimize absorption, and the size of the window is often reduced to avoid decreasing stack pressure as much as possible.

In the case of SAXS (small angle X-ray scattering), some cell designs used for conventional diffraction can be used and flat cell geometry is not an issue, as the angular range is very limited and hence the X-ray path is almost identical for all scattering angles measured. The main concern is to avoid window materials which can contribute to the signal and hence materials not having long range structural order (polymers or glassy carbon) cannot be used in this case. Care has to be taken in choosing window materials not exhibiting Bragg peaks in the detector range. To this purpose, often aluminium or mica is used.

Some cell set-ups can be employed for different techniques (*e.g.* diffraction and XAS) and facilitate complementary studies (multi-modal characterization), while in other cases, specific geometries are required (*e.g.* cylindrical or radially symmetric cells for tomographic imaging). Customized cell setups were common in the early days of *operando* studies and new improved designs are being continuously developed[8] considering adaptability to somewhat different concepts (*e.g.* all solid state cells). Yet, a gradual evolution to more standardized configurations has taken place,[9–11] with high energy experiments allowing measurements on conventional setups (pouch, coin and cylindrical). An interesting approach to enable the use of these cells with lower beam energies is to modify them, such as laser thinning the top coin case to 50 µm. This has enabled an *operando* long duration ageing study for >100 cycles by simply testing the cell continuously in the beamline hutch and periodically placing it under the beam.[12] Conventional setups enable improved representativity with respect to real commercial cells, but they may be limiting in some cases (*e.g.* spectroscopy cannot be

performed unless suitable windows are implemented). Overall higher flexibility can only be achieved for specifically designed setups[13–15] and can also pave the way to multimodal characterization coupling different techniques. These on purpose developed cells can allow the use of a third electrode, for independent monitoring of the potential at the positive and negative ones, opening also the possibility of performing electrochemical impedance spectroscopy on a single electrode.[16] Regardless the type of cell, the high flux of synchrotron radiation allows fast data collection and thus it enables high-throughput experiments measuring multiple cells, and for this, special sample holders have been designed.[13,15,17]

Sample preparation is another relevant aspect, whose importance is not always emphasized.[10] First of all, non-active cell components (such as binder, carbon and electrolyte) do bring in a contribution, *e.g.* background increase at low diffraction angles due to scattering by an amorphous carbon additive, the position of which is dependent on the electrolyte.[18] Metal current collectors (typically Cu and Al for negative and positive electrodes in the Li-ion technology) will also result in sharp peaks in diffraction studies, which can mask the evolution of some overlapping peaks corresponding to the sample under study. The collector of the same element of investigation in the counter electrode is hiding the information obtainable by XAS, and a hole in the collector in correspondence with the beam path can be foreseen to avoid the overlapping signals. The total absorption of a cell (considering windows, electrodes, separator, and electrolyte) needs to be adjusted in the case of XAS measurements in transmission mode to minimize the total absorption by approaching an absorption jump of 1 for the element of interest. In particular, *operando* XAS at relatively low energies needs to minimize the X-ray absorption along the beam path and are often more accessible in fluorescence mode. For S K-edge *operando* XAS studies, for example, S compounds have been embedded in a Cu mesh to allow the penetration of the X-ray beam.[19] Electrode preparation mimicking commercial protocols is *a priori* desirable (*e.g.* tape casting), as electrochemical performance will be improved. Yet, this can be a drawback for fundamental studies on the redox mechanisms of specific materials with particles exhibiting a morphology prone to preferential orientation (*e.g.* TiS_2 platelets).[18] In such a case, simple mixtures of the material with carbon black will be preferred to enable the observation of *00l* reflections.

Although common battery technologies use liquid (either aqueous or organic solvent based) electrolytes, the development of batteries using solid electrolytes is currently a hot topic. Indeed, concepts involving lithium metal as the negative electrode would *a priori* enable very high energy densities and improved safety with respect to state-of-the-art Li-ion technology. The use of solid electrolytes brings about additional parameters to consider for *operando* experiments such as the need to maintain external pressure.[20]

Besides the control of pressure, efforts are also currently underway to extend experiments beyond ambient conditions. Their interest arises from the need to understand the influence of temperature in the redox mechanism. They can bring in relevant data regarding real battery operation under very different environments as temperature will impact kinetics and can also induce phase transitions within the electrodes. Moreover, these studies can also provide inputs on temperature driven degradation reactions. In effect, cycling to temperatures of up to 70 °C is a common means to accelerate ageing phenomena in batteries.[24] Ideally, the cell designs should not differ much from those used at room temperature to ensure the representativity of the electrochemical behaviour. The main issue in this case is to be able to heat/cool the cell to a homogeneous and controlled temperature. Note that the thermal expansion of the unit cells of the materials under study does also need to be considered and that it provides a suitable indirect way to calibrate the cell temperature. While heating could be *a priori* easier *via* an electrical resistance, interference with the electrochemical response cannot be excluded. Since a crucial aspect is ensuring that the probed sample (and not only the housing) is thermalized, a circulating fluid inside the cell body appears as the most attractive option enabling both heating and cooling (Fig. 2). Other options could be to work

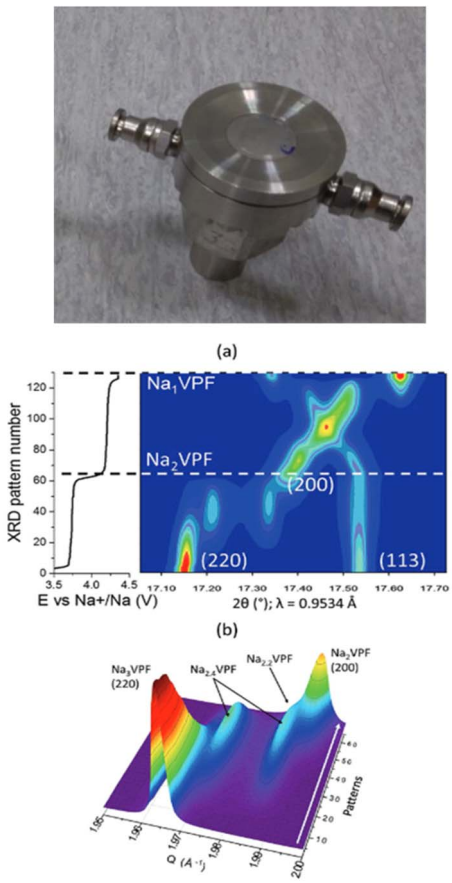

Fig. 2 Image of a thermalized cell[21] designed taking the one reported in ref. 22 as the basis, modified to enable fluid circulation through the main cell body (top). Diffraction patterns achieved using a similar setup for $Na_3V_2(PO_4)_2F_3$ in sodium cells at C/10 and 0 °C, which enabled the phase diagram to be followed upon Na^+ deintercalation in 2D (a) and 3D (b) plots. Reproduced from ref. 23 with permission, © WILEY-VCH Verlag GmbH & Co.

with cylindrical cells, which could be placed inside a cryostat or a hot blower, as in this case the geometry would enable the combination with other techniques, such as tomography.

In addition to the generic interest in elucidating the influence of temperature in the redox mechanism, these experiments may be even more relevant in specific battery technologies operating at high temperature, such as Li metal solid polymer electrolyte cells, commercialised using $LiFePO_4$ as the positive electrode, which operate at *ca.* 80 °C.[25] In this case, a capillary cell setup was used, wrapped in a heating band, which enabled the control of temperature and spatially resolved phase distribution. The results allowed inferring the differences between the structural changes taking place close to the electrolyte and those occurring in the vicinity of the current collector. With respect to cooling, the study of the redox mechanism in graphite electrodes at 0 °C has also been reported, with the stage sequence observed being different from the one taking place at room temperature, which is relevant to understand the behaviour of Li-ion cells in cold climates.[26] Experiments at different temperatures may also be relevant for new battery technologies, for instance, experiments down to −40 °C cooling pouch cells with liquid N_2 were carried out to get further insights into the intercalation of chloroaluminate in graphite electrodes in aluminium batteries.[27]

Elastic scattering based techniques

Diffraction

X-ray powder diffraction appears as the most mature *operando* X-ray based analysis technique within the battery field. The first report dates back to 1978 using a specially designed cell with a CuK_α radiation laboratory diffractometer.[28] This technique spread quickly in the last few decades concomitant with the development of various cell designs, some becoming commercial, and continuous improvements of laboratory diffractometers (higher energy derived from MoK_α or AgK_α radiation and higher throughput related to the use of rotating anodes and solid-state position sensitive detectors).

Since most battery electrode materials are crystalline, powder diffraction can provide time-resolved information on the evolution of the phase composition (*e.g.* formation of solid solutions and phase transitions), the average crystal structures (variations in the cell parameters, (de-)inserted ion localization in the crystal structure and site occupancy) and the microstructure (micro-strains and coherent diffraction domain size) occurring during the redox reactions involved in battery operation. The emergence of synchrotron and dedicated instrumentation (optics and experimental station) expanded the range of operation by increasing the flux on the sample, contributing to a better signal-to-noise ratio and also enabling a much faster acquisition time. The former allows spotting of weak peaks, which can enable the detection of otherwise elusive phases induced by ion ordering[29,30] or the formation of incommensurate structures.[31] Faster acquisition opens the possibility to perform experiments at much higher rates such as 60C (ref. 32) but more importantly, it pushed towards the development of high throughput setups for serial data acquisition on several batteries operating in parallel.[17,33] Indeed, intermittent sample probing enables following several cells simultaneously (which usually offers enough data points, unless the aim is to follow short-lived intermediates), while at the same time reducing beam exposure and hence minimizing potential beam damage. In addition to that, fast data collection can be used as a mesh mapping tool in a single cell for tracking inhomogeneities (see below).

Better energy and angular resolution should enable a more accurate refinement of the crystal structures of the phases observed from the data collected *operando*.[33] In addition, energy tunability enables optimizing the powder diffraction conditions (operate in transmission and minimize absorption by the cell casing), while also offering the possibility to couple powder diffraction and hard X-ray absorption techniques.[34]

The emergence of high energetic and high brilliance 3rd generation synchrotron sources, together with improved optics (Kirkpatrick–Baez mirror setups and refractive lenses), has made possible to standardly decrease beam sizes, in the micrometer range first, and ultimately down to the diffraction limit in the very hard regime (<20 nm at ∼100 keV). These conditions open the way to *operando* XRD microdiffraction, which was typically used to study the phase evolution of individual $LiFePO_4$ nanoparticles and provided fundamental insights into the rate dependence of the redox mechanism for this compound, widely used in commercial cells.[35] In this case, the small beam illuminated a finite number of grains whose Bragg reflection spots could be discriminated. This approach has recently enabled following the lithium concentration across a 80 μm thick graphite electrode, detecting and quantifying heterogeneities.[36] One step further consists in probing a single particle using XRD-tomography based techniques allowing the visualization of cracks and strains in $LiNi_{0.8}Mn_{0.1}Co_{0.1}O_2$ induced during battery operation and contributing to capacity fading.[37]

Most often experiments in a synchrotron are carried out in transmission mode, with the incident beam along the electrode stacking direction. While this enables simpler alignment of the cell, it prevents the detection of inhomogeneities, which can arise in thick electrodes and are relevant in commercial batteries, especially at high operation rates. A possible alternative is to direct the beam parallel to the battery layers, in grazing incident geometry.[38] This geometry enables tuning energy and/or changing the incident angle and can be useful for depth profiling experiments. This can be extremely useful to get a better understanding on how electrochemical reactions propagate but additional considerations apply as misalignment effects can easily interfere with the interpretation of results. Probing the electrode material at different cell locations and depth profiling are also possible using a pencil size beam coupled to energy dispersive diffraction.[39,40] In this case, specific detectors able to discriminate energy are required and data treatment is also somewhat more complex but the advantage is that the probed volume, defined by incoming and scattered beams, remains constant, which is particularly valuable when dealing with very small beams.

The maturity of the *operando* X-ray diffraction approach does also manifest in the development of multimodal approaches coupling it to other complementary techniques (often also *operando* and hence using cell setups compatible with both). A meaningful illustration of this methodology is the combination of energy dispersive diffraction and X-ray tomography, which have enabled the visualization of the degradation of the InLi alloy electrode/$Li_{10}SnP_2S_{12}$ electrolyte interface in all solid-state cells[41] and to get further insights into the mechanism of anion intercalation in aluminium cells using graphite positive electrodes.[42]

With the improvement of synchrotron facilities, experiments at high energy (~80 keV) have enabled penetration depths on the order of 1 mm with very good spatial resolution (ultimately related to focusing optics). One of its main advantages is the possibility to use real commercial cells in the experiments, such as pouch $LiNi_xMn_yCo_{1-x-y}O_2$/hard carbon[44] or 18650 $LiFePO_4$/graphite for which phase transitions at both electrodes could be followed at a relatively fast rate (4C).[45] In the former case, the lattice expansion of the Cu current collector enabled measuring the temperature and probing different regions of the cell allowed the drawing of 2D maps, which despite limited spatial resolution (0.3 mm, beam size) facilitated the detection of inhomogeneities (see Fig. 3). Last but not least, it is also worth mentioning that recent *operando* studies under optimized conditions at 107.7 keV (0.1173 Å) have permitted to follow the homogeneity of the lithium plating/stripping process in an "anode-free" pouch cell despite the low scattering factor of lithium.[46]

Pair distribution function analysis (PDF)

Besides diffraction, involving only Bragg scattering and hence providing long-range average structural information, the consideration of total scattering (including also diffuse scattering) and the corresponding pair distribution function (PDF) provides local information. It describes the probability of finding two atoms separated by a certain distance in the material under investigation, which is particularly useful to characterize systems in which no long-range order exists, and hence diffraction is not an option. Information deduced from PDF can also in some cases[13] complement results achieved with SAXS (see the next section). This technique can be also considered complementary to extended X-ray absorption fine structure (EXAFS), in which the local structure is probed around an absorber (see the corresponding section).

In order to achieve data over a relevant range of momentum transfer (Q) to reach low r values, high energies (>45 keV) and large angular coverage of the detector are required, which are only available in some specific beamlines. Otherwise, the situation would be similar to laboratory X-ray sources for which the energy is limited (maximum 25 keV with an Ag source) and the flux much lower. Nonetheless, despite these issues, Pair Distribution Function analysis is being increasingly used.[47] Its result is a histogram of pair distances in the real space, but Fourier transformation is required due to data being collected in the reciprocal space. *Operando* total scattering experiments

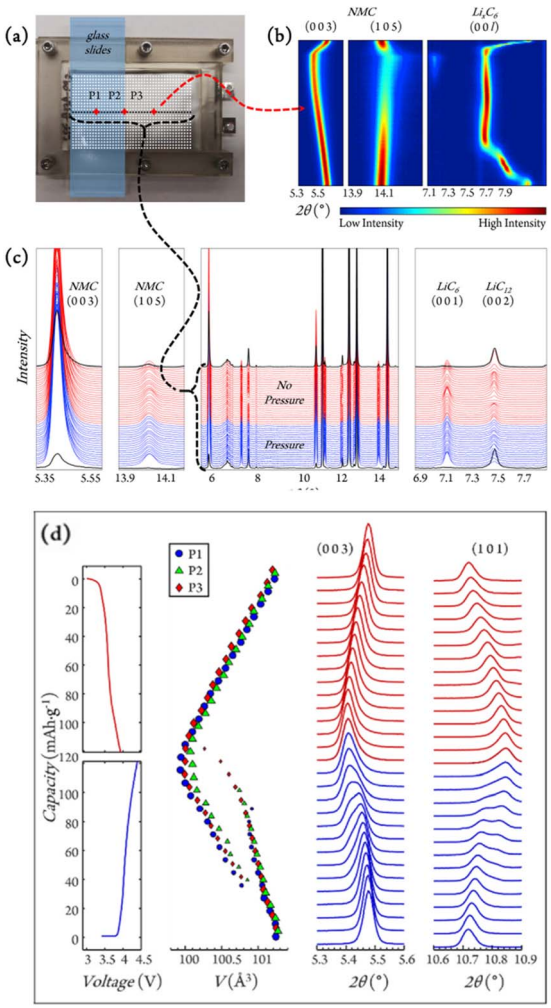

Fig. 3 (a) Experimental setup for *in situ* grid mapping (white dots) and *operando* position tracking (red diamonds: P1, P2, and P3) for graphite/$LiNi_{0.5}Mn_{0.3}Co_{0.2}O_2$ (NMC532) single layer pouch cells. (b) Contour plot for NMC532 and Li_xC_6 reflections of interest collected at P3 during charge and discharge. (c) Diffraction line scan across the pressure interface (black dotted line in (a)). (d) The evolution of voltage during the 10th cycle together with selected NMC peaks and cell volumes, with marker sizes indicating phase fractions. Reproduced from ref. 43 with permission, © Elsevier.

are challenging because a low, constant and reproducible background is required to extract reliable data, and this makes the cell design much more critical than for diffraction, which focuses on sharper Bragg peaks.[48]

This technique does also place additional requirements on the cells to be employed. If using high energy radiation and a small sample to 2D detector distance (typically 100 mm), flat cells will result in different absorption at high angles and thus a cylindrical geometry is more suitable. In addition to that, a blank cell needs to be measured to remove its contribution. Data treatment can also be complex. The small box modelling approach requires the crystal structure as an input and then the B (Debye–Waller) factors or selected atom positions can be refined. Discrepancy in PDF calculated values with respect to the average crystal structure can be attributed to local effects

such as slight variations of bond distances. Another possibility is big box modelling including all atoms in a given volume and adjusting their positions to match the experimental data. Yet, this is only viable for small nanosized particles with a limited number of atoms and involves a significant computing time.

Overall, besides the limitations explained above, the experimental setup is not significantly different from that of conventional powder diffraction, and both depth profiling or combination with other techniques (*e.g.* tomography)[49] are also possible. Nonetheless *operando* PDF insights are especially valuable for materials with a disordered crystal structure for which diffraction cannot provide information. Besides innovative materials, such as transition metal oxides with a disordered rock salt type structure used as positive electrodes in lithium ion cells,[48] one particularly interesting case is non-graphitizable hard carbon, which has a structure consisting of graphene nanosheets with significant turbostratic disorder. Hard carbon is the negative electrode material of choice in sodium-ion batteries, a technology being already in the manufacture phase by several start-up companies and subject of intensive study. In this case, despite the difficulties in finding a suitable structural model and the overlaps from scattering by the electrolyte,[50] meaningful data could be achieved which enabled to correlate pyrolysis temperature with the presence local structural defects and the electrochemical performance while also shedding light on the currently controversial redox mechanism.

Small angle X-ray scattering (SAXS)

Small angle elastic X-ray scattering enables probing bulk microstructural features in a range of 1–300 nm (*e.g.* microporosity and particle size), which provide signals at very low angles (typically below 1°) when compared to diffraction. As in the case of diffraction laboratory equipment is available, the benefits of synchrotron radiation being that the higher flux enables much faster experiments, which may be relevant to get a deeper understanding of kinetic aspects. It also enables accessing longer lengths, so that some Bragg peaks can be observed if the sample is crystalline and hence complementary information can be achieved (note that this is sometimes also termed WAXS, Wide Angle X-ray Scattering to stress its contrast with SAXS). This technique can be used to study the pore dynamics during redox operation in low crystallinity electrode materials, such as hard carbons. Yet, data treatment is not straightforward and requires not only evaluation and subtraction of the cell component contributions but also the use and validation of reliable models and sophisticated data analysis.[51] When SAXS-WAXS combined experiments are carried out, two detectors are used, one collecting the SAXS signal and the other the Bragg diffraction (with a limited angular range and hence not suitable for crystal structure determination). An additional issue is that given the need to access large *d* spacing values, X-ray energies in the medium range are most suitable (*e.g.* 10 keV), and hence absorption from the sample can be a problem.

This technique has been useful in probing reaction mechanisms both in materials which are already at the commercialization scale (or close to) for the Li-ion technology (*e.g.* silicon–graphite based composites as negative electrodes)[52,53] and also in the mechanistic study of alternative chemistries such as the Li–O_2 concept.[54] In the former case, monitoring the silicon particle active volume by SAXS concomitant with the stage formation in graphite inferred from WAXS enabled the degree of lithiation in each component (affected by the cycling rate) to be independently followed, and also the assessment of the effect of pre-lithiation. In the latter, the growth mechanism of Li_2O_2 upon oxygen reduction in weakly solvating electrolytes is investigated, with results seemingly dismissing previous beliefs about the formation of a passivating conformal Li_2O_2 film which would intrinsically limit the achievable electrochemical capacity.

Absorption and emission based spectroscopic techniques

Absorption spectroscopy

The application of XAS to materials science was for many years overshadowed and underestimated when compared to X-ray diffraction techniques. This was due to both XRD enabling precise crystal structure determination and the lack of extremely bright X-ray sources required to accurately determine the X-ray absorption coefficient of a material as a function of photon energy. Major advancements in the theory for extended X-ray absorption fine structure (EXAFS) triggered the need for dedicated storage rings that led to the construction of the first synchrotrons during the decade of the 80's.[55,56]

A great advantage of XAS is that it is element specific and probes short-range order, giving structural and chemical information of not only crystalline samples but also amorphous materials, liquids, gases, and complexes in solution, including highly diluted systems. The X-ray absorption near-edge structure (XANES) range of the spectrum corresponds to the electronic configuration and it is sensitive to the oxidation state of the element. Moreover, as the excitation energy is just sufficient to allow the photo-ejected core electron to reach the continuum, the photo-ejected electron wavelength is relatively large with respect to the interatomic distances, and the global XANES shape can be used as a fingerprint of chemical species. Instead, the EXAFS region of the spectrum corresponds to photo-ejected core-electrons of relatively high energy, with wavelengths comparable to the interatomic distances. In this region, the EXAFS oscillations can be modelled in the single scattering approximation obtaining quantitative information on the interatomic distances, kind and number of atoms surrounding the absorber and their relative disorder. Typically, EXAFS studies are performed at room temperature, for example as a function of state-of-charge, to access information on the charge compensation mechanism. Interesting complementary information can be achieved by *ex situ* temperature dependent EXAFS studies. Such measurements allow the local bond strength and structural disorder to be quantitatively accessed, both parameters affecting the final electrochemical properties. In particular, the local bond strength depends on the absorber-ligand orbital overlap, which affects the redox process. In this

sense, it has been recently proposed that a larger degree of overlap between the transition metal and oxygen electronic states in Li-rich NMC increases the rigidity of the oxygen sublattice upon lithium deintercalation and results in a more reversible oxygen redox.[57,58] Following the evolution of the EXAFS oscillations as a function of the temperature enables the experimental elucidation of changes in the local structure resulting from the redox process. Moreover, low temperature EXAFS data allow the quantification of the static disorder, which affects the diffusion coefficients of the intercalating ions. For instance, both local static disorder and bond strength have been found to influence capacity in Na_xCoO_2.[59]

Whenever possible, XAS spectra are recorded in transmission to achieve a higher signal-to-noise ratio. This allows for a fast scanning speed and is bulk sensitive, as the beam crosses the full sample or cell. In contrast, fluorescence acquisition mode shows typically lower signal-to-noise ratios and requires slower scanning speeds. It is used to investigate non-X-ray transparent samples or highly diluted systems.[60] Alternatively or complementarily, XAS measurements in total electron yield (TEY) mode benefit from a high signal-to-noise ratio, fast scanning speed and surface sensitivity. The fundamental principles of the XAS method and progress of the instrumentation as well as the data analysis of both XANES and EXAFS have been covered in detail in several recent reviews such as ref. 61 and 62.

Hard X-ray. Hard X-ray XAS enables the monitoring of the chemical and structural changes taking place during redox processes. It has been extensively applied *operando* to the study of battery materials since the early 90's with pioneering investigation of alkaline MnO_2 batteries[63] and organosulfide polymeric electrodes for Li and K ion technologies.[64] One of the main reasons why this technique has been so widely used in the battery field is related to the fact that it is element specific and the most common electrode materials contain first-row (3d) transition metals as redox centres, with K-edge energies lying between 4.5 and 10 keV which is of easy access. In addition, the large penetration depths in the hard X-ray range allow the bulk of the material to be probed and the measurements can be made in transmission mode. Several studies have enabled the unveiling of the charge compensation mechanism and local structure evolutions taking place during electrochemical delithiation and lithiation of layered oxides in general and in materials containing more than one active redox element in particular, such as NMCs. Early studies following the XANES of the K-edge of Ni, Co and Mn in the operating voltage (up to ~4.6 V) enabled the conclusion that manganese remains as Mn^{4+} and that the charge compensation mechanism involves mainly the oxidation of Ni^{2+} to Ni^{4+} ions.[65] The element specificity of XAS enables pinpointing which of the potentially redox active elements undergoes oxidation or reduction at each state of charge and has enabled recently the understanding of the underlying anionic redox process that governs the hysteresis and kinetics of Li-rich electrode materials such as $Li_{1.2}[Ni_{0.13}^{2+}Co_{0.13}^{3+}Mn_{0.54}^{4+}]O_2$[66] and Li_2RuO_3.[67] In addition to that, EXAFS provides quantitative information on the local structure around an absorber, enabling to directly access local strains and vacancies and hence is an ideal complement to diffraction data. Numerous examples of *operando* XAS studies on the electronic and structural properties of active electrode materials can be found in specific literature[60,68–73] and reviews.[62,65,74]

Experimental advances and improvements of synchrotron radiation sources lead to the development of Quick scanning EXAFS (QEXAFS), which pushed the acquisition time of a single spectrum in real-time from tens of minutes down to the sub-second regime. It has become an ideal tool for *operando* investigations of the kinetics of electrochemical reactions in batteries.[77] The sub-second QEXAFS technique is based on specialized X-ray monochromators, which enable rapid and continuous energy scans by smoothly oscillating the monochromator crystals.[78,79] The achievable temporal resolution is limited by the mechanical stability of the monochromator, the response times of the detectors, and the available photon flux. QEXAFS has been employed to study nonequilibrium phase transitions in $LiNi_{0.33}Mn_{0.33}Co_{0.33}O_2$ at high rates, enabling to determine that the redox process on Ni ions occurs to a larger extent at higher C rates, which is consistent with the benefits in rate capability observed for high Ni content materials (Fig. 4a).[75] XAS has also been used to investigate transition metal high-entropy oxides (HEOs), a class of conversion-type electrode materials studied for Li-ion batteries that integrate at least five elements into a single phase to increase the configurational entropy, which is expected to improve electrode reversibility and cycle life. The reaction products of these HEOs are nanometric, defective and poorly crystalline and thus difficult to probe *via* XRD. The complex charge storage mechanism of spinel type $(CrMnFeNiCu)_3O_4$ HEOs has been unveiled by *operando* quick XAS enabling to confirm that all five elements contribute to the charge capacity to different extents at each state of charge, the processes being in some cases non- or poorly reversible, especially the reoxidation of Cu^0 to Cu^{2+} (Fig. 4b).[76]

Soft and tender X-ray. Compared with hard X-ray, soft X-ray absorption spectroscopy (sXAS)[80] is a more direct and efficient experimental probe of the electronic states near the Fermi level. sXAS is typically measured in TEY, accessing surface sensitivity (a few nm). When the soft X-ray fluorescence yield (FY) is simultaneously available, as in the harder X-ray regime, it allows surface and bulk contributions to be discerned. However, the short penetration depth of soft X-rays requires dedicated *operando* set-ups designed to operate in high vacuum environments. Strategies to overcome the vacuum requirement are for instance the use of cells with integrated X-ray transparent windows (Si_3N_4, SiO_2, Si or graphene) or making perforations on the current collector, which enabled *in situ* measurements on NMCs and $LiFePO_4$ electrode materials.[81] Another original approach deserving mention is the intentional generation of a gas bubble from the electrolyte inside a microfluidic electrochemical cell with high intensity X-rays, which enabled the study of the solid electrolyte interphase (SEI) on silicon electrodes *in situ* through transmission soft XAS (Fig. 5).[82] Last but not least, the development of frequency modulated methods enabled decoupling and measuring the tiny TEY current generated by the secondary electrons at the electrode/electrolyte interface from the current circulating through the working electrode under

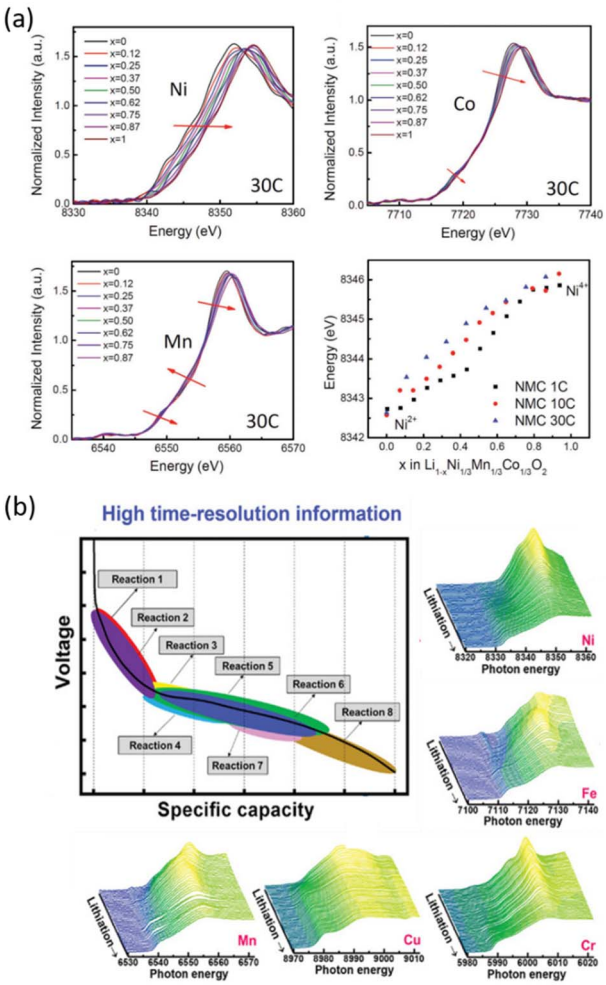

Fig. 4 Two examples of *operando* quick-scanning XAS: (a) XANES results of $LiNi_{0.33}Mn_{0.33}Co_{0.33}O_2$ at Ni, Co, and Mn K-edges throughout oxidation at a 30C rate. Ni K-edge energy shifts as a function of nominal lithium content *x* in NMC during oxidation at different rates (1C, 10C, and 30C). Reproduced from ref. 75 with permission ©John Wiley&Sons. (b) Voltage *vs.* capacity profile for the $(CrMnFeNiCu)_3O_4$ HEO electrode, and corresponding XAS spectra which enable changes in the oxidation state/coordination for the involved metal ions to be inferred as a function of the electrode state of charge.[76]

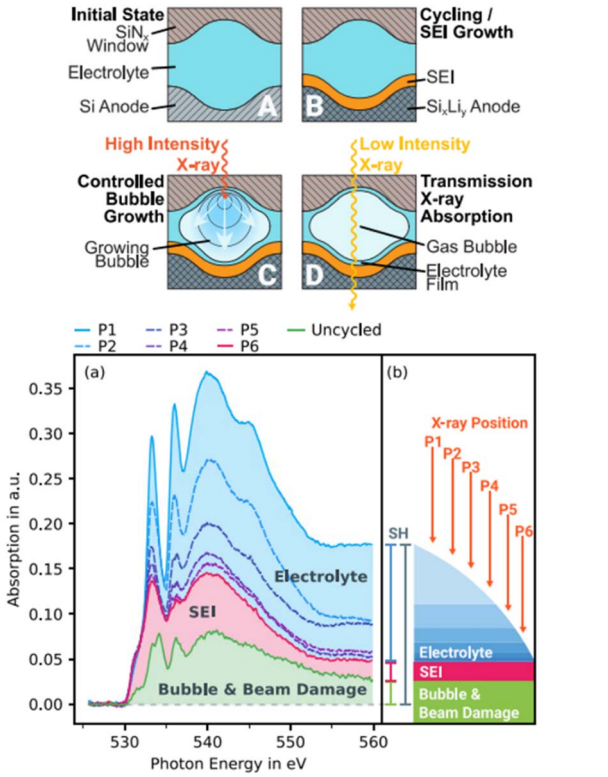

Fig. 5 (a) Illustration of a novel approach to investigate the SEI on silicon thin-film electrodes *in situ* through transmission sXAS and (b) extraction of the SEI spectrum from the overshadowing electrolyte spectrum and subtraction of the bubble and beam damage.[82]

electrochemical cycling, providing a platform to investigate solid/liquid interfaces by *operando* sXAS.[83,84]

The tender X-ray (TX) range, in which the K-edges of several relevant elements used in batteries, such as Na, Mg, Al, Si, and P, are located is unfortunately not commonly accessible. Indeed, it is often too high for sXAS beamlines and too low for most hard X-ray XAS beamlines. However, the penetration depths are longer that those of soft X-rays, so that conventional coin cells can be employed for *operando* measurements provided that the window is thin and composed of light elements, with Be, Si_3N_4 or Kapton being the most commonly used. On the other hand, the attenuation length is too low to measure in transmission mode and therefore FY is preferred.

Operando XAS on Li/S or Na/S batteries[19,85,86] has shed light on sulfur speciation during the redox process and on the mechanisms that govern dissolution and deposition processes (Fig. 6). The different polyanionic species formed during cell operation are easily distinguishable by linear combination fits (LCFs) as their absorption edges. Spatially resolved XAS has been used to differentiate between the intermediate species present in the positive electrode and the separator of an operating Li/S cell during the first and second cycles[87] and time-resolved *operando* XAS experiments with sub-second time resolution provided insights into the effect of the discharge rate in the redox mechanism.[88] Finally, it is also worth mentioning that P K-edge XAS on $LiFePO_4$ electrodes could also be followed *via operando* TX-XAS.[89]

In addition to the absorption techniques mentioned above which are based on electronic transitions to unoccupied states, X-ray emission spectroscopy (XES) is especially suited to probe the occupied states, including the valence electrons. Probing emission lines one can infer not only on the emitter's oxidation and local spin state, but also on the ligand nature. Studies combining XES and XAS revealed that Mn^{3+}/Mn^{4+} play an active counterbalancing role during oxygen redox reactions in lithium- and manganese-rich layered oxides.[90] *Operando* XAS enables also multi-technique approaches combining XANES and EXAFS with sXAS, XES, and even other inelastic scattering techniques, such as resonant inelastic X-ray scattering (RIXS) or X-ray

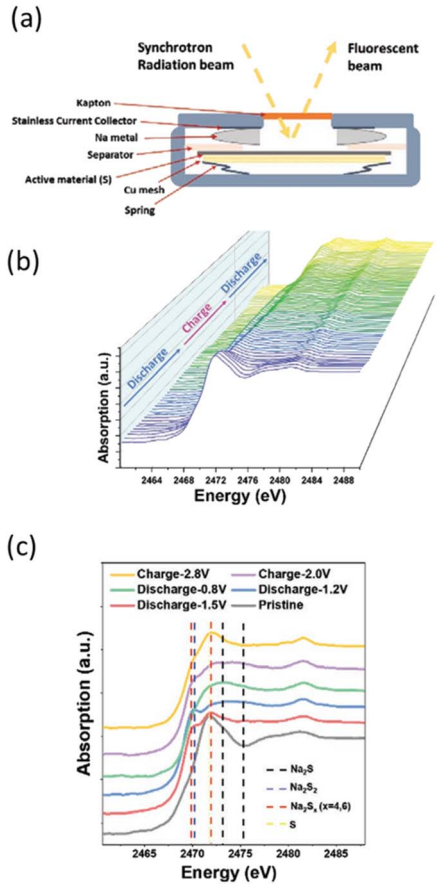

Fig. 6 (a) Scheme of coin cells allowing measuring S K-edge *operando* in fluorescence mode. (b) Sulfur K-edge XANES evolution as a function of the state of charge followed *operando* in Na/S batteries and (c) selected spectra at various states during the first cycle with positions for reference compounds highlighted by vertical dotted lines. Reproduced from ref. 19, © John Wiley&Sons.

Raman scattering (XRS), the latter giving access to soft X-ray absorption edges by exploiting hard X-rays, *i.e.* with bulk sensitivity.[74] Complementary studies involving sXAS and RIXS were especially useful to probe light elements such as oxygen. This enabled the correlation of the mechanism of generation of O^{2-} and dimerization to form $(O_2)^{n-}$ with the localization of electrons–holes primarily on the oxygen atoms in $Li_{1.2}Ni_{0.13}Co_{0.13}Mn_{0.54}O_2$. By investigating the local environment around the transition metal ions using XANES it was evidenced that Mn^{4+} plays a specific role in trapping the holes on the oxygen atoms that ultimately determine the fine balance between oxygen loss and reversible oxygen redox in the operation of these electrode materials.[66]

Photoelectron spectroscopy

Photoelectron spectroscopy is a well-established technique for surface analysis that has become widely applied for the determination of the chemical environment for the different elements present in a sample. Although mostly indicated for studying surfaces, its widespread availability at the laboratory scale has resulted in its use to determine the redox state of transition metals, despite its lower reliability to probe the bulk when compared to XAS in transmission mode.[91] Among the techniques considered in this perspective paper, this is the only one based on the detection of electrons instead of photons. It originates from the photoelectric effect, the emission of electrons with kinetic energy E_{kin} after irradiation of photons with energy $h\nu$, according to the conservation of energy:

$$h\nu - E_{kin} = E_{fin} - E_{in} = BE + \Phi \quad (1)$$

where h is the Planck constant, and E_{fin} and E_{in} are the final and initial energy of the sample, whose difference for solids is conventionally split at the Fermi energy into a Binding Energy (BE) and a work function (Φ). The BE is an intrinsic property of the electronic structure of the investigated compound, while the work function is sensitive to its surface electric dipoles. The number of electrons as a function of their kinetic energy essentially reproduces the shape of the density of electronic states (DOS). It is important to stress that binding energy shifts in XPS may be not only of chemical, but also of electrostatic origin,[92] when a dipole exists between an atom and the sample ground. Thus, for the correct interpretation of shifts when non-electron conducting layers are involved (such as electrolytes in *operando* experiments), the cell configuration must be taken into account.[93]

Since the right part of eqn (1) is determined by the material, the actual E_{kin} range is controlled by the chosen $h\nu$ photon energy. While electrons interact with any atom following a universal curve,[94,95] the penetration depth of X-rays strongly depends on the elements they interact with, in particular when they are specifically absorbed to excite transitions. Nonetheless, the electron inelastic free mean path tends to be much shorter than the penetration depth of X-rays of the same energy (1 nm at 500 eV and 10 nm at 10 keV). Even in gaseous phases, the free path is short, and therefore for sufficient electron collection either ultra-high vacuum (UHV) or short paths at higher pressure are necessary. The availability at synchrotrons of hard X-ray photoelectron spectroscopy (HAXPES) has significantly expanded the sampling depth, overcoming some of the important limitations of lab-scale XPS. In fact, the high surface sensitivity makes challenging even *ex situ* characterization. Surfaces are easily affected by interaction with the atmosphere and adsorbates or reacted surface layers need to be removed after introducing the sample in a vacuum by either heating or gas sputtering with an ion gun. Even when applied carefully, such methods will hardly leave an exact representation of a fresh surface of the electrode material that may be of interest. For the same risk of altering composition and redox states, caution must be used in depth profiling studies assisted by sputtering.[96] The non-destructive depth profiling offered by varying the photon energy with a synchrotron source is particularly attractive, as the electrode surface is often the subject of interest (investigation of passivation and SEI layers, which may exhibit a complex composite gel-like structure). In these cases, manipulation may still largely affect surfaces, and ensuring representativity is not straightforward. To exclude the impact of environmental contamination, the integration of chambers

enabling to perform electrochemical experiments and handle samples directly connected to the analyzer chamber has been proposed.[97] However, introducing surfaces wet with complex organic/inorganic mixtures directly into a vacuum poses a problem to the SEI integrity. Near ambient pressure photoelectron spectroscopy (NAPP) has mitigated this problem. By differential pumping, it is possible to keep a higher pressure close to the sample surface, so that fast drying is avoided, and the liquid electrolyte can be measured during hours simultaneously to the solid electrode.[98] Other approaches for SEI analysis have addressed the formation of electrochemical interfaces by *in situ* (UHV) step-by-step deposition of solid electrolytes on top of electrode materials, which allows the study of dipole formations by following the shifts of the characteristic peaks of the substrate and electrolyte.[99] *Operando* XPS experiments would eliminate the effects of variable ambient contamination, but are more difficult to envisage. To observe effects comparable to the application of a bias, the charging produced by irradiation of an electron gun has been exploited to generate a so-called "virtual electrode"[100] and explore interactions between metallic lithium and sulfide solid electrolytes. The most straightforward option for truly *operando* photoemission measurements is using solid state cells. One early example was based on a Na β″-alumina plate to study the electronic effects of Na intercalation on a top layer of *in situ* prepared TiS_2.[101] More recent work studied the reactivity to oxygen of RGO deposited onto a solid glass-ceramic NASICON-type electrolyte in an ambient pressure XPS chamber. The resulting solid-state Li/O_2 battery positive electrode demonstrated the intrinsic instability of most carbon defects to the oxygen radicals.[102] Some *operando* studies with laboratory XPS could reveal chemical and electrochemical degradation at the interface between the two components of the electrode and sulfide solid electrolyte.[103–105] The method is based on the observation of an electrode fabricated as a composite between the electrode active material and the solid electrolyte, so that both components and their interface are observed simultaneously. However, with the availability of HAXPES, it is now possible to study full solid state batteries. With a 10 nm Al collector on top of a 35 nm $LiCoO_2$ layer, the P 1s signal of the garnet solid state electrolyte beneath the positive electrode could be observed, in addition to the signal of the remaining elements Al, Li, Co, and O.[106] With liquid electrolytes, the feasibility of cells containing ionic liquids has been demonstrated in UHV.[107] Instead, the use of more conventional organic or aqueous electrolytes is still limited, although technical advances have been possible with the introduction of graphene windows for the observation of liquids[108] and the availability of liquid flow cells supporting graphene or Si_3N_4 windows that with a typical thickness of 25–50 nm can be crossed by electrons emitted from harder X-rays.[109] Such experiments are becoming frequent especially in catalysis.[110] Another approach for liquid electrolytes, requiring NAPP, is the "meniscus XPS" or "dip and pull" method.[111] It consists in pulling the electrode out of the electrolyte so that it forms a nm-thick layer. These configurations are depicted in Fig. 7. Examples of experiments involving liquid electrolytes are still scarce, mainly because of the limited

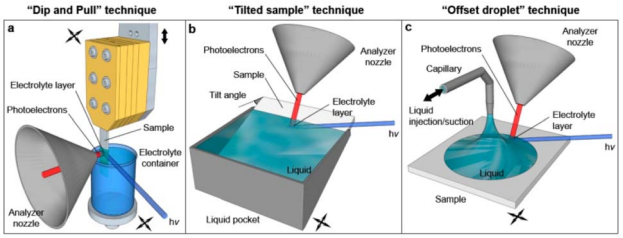

Fig. 7 Schematic representation of the original dip-and-pull method (a) and two variants (b and c) for XPS analysis of solid–liquid interfaces. Some of the electrons generated at the interface cross the liquid meniscus and are collected by the analyzer. Reproduced from ref. 116.

availability of beamlines capable of HAXPES and near ambient conditions. One example is the HIPPIE beamline at the MAX IV laboratory that is designed for *in situ* and *operando* NAPP experiments at the solid–liquid (dip-and-pull setup) interfaces under full electrochemical control.[112,113] In addition, the radiolysis problems, discussed in the imaging section, represent a major challenge.[114] As for other spectroscopic methods, the imaging mode has also been demonstrated *operando*, enabling for instance differentiation of lithium extraction rates from different facets of 10 μm $LiCoO_2$ single particles, suggesting that the electrode rate capability can be improved by controlling the crystal habit.[115]

Most of these studies are facilitated by tender and hard X-rays with higher penetration depths (several tens of nm), enabling *operando* experiments under more realistic conditions in terms of electrodes and electrolytes. On the other end, the use of soft X rays, even if increasing the surface sensitivity, allows much higher sensitivity to the lightest elements, including lithium, whose photoionization cross section is weak with laboratory radiation.

Infrared spectroscopy

Fourier transform infrared (FTIR) spectroscopy is based on the absorption of infrared light by the molecules present in the sample of interest. It is a non-destructive technique (photon energy < 1 eV) and particularly useful for non-crystalline organic compounds for which absorption occurs when the frequency of the incident IR light coincides with the vibrational frequency of a bond. Infrared spectra can thus constitute a fingerprint for some of the components of electrolytes, the SEI and organic electrode materials. *Operando* measurements would therefore enable the investigation of not only the evolution of the cation solvation structure in the electrolyte[117,118] but also the redox mechanisms and/or degradation processes for organic electrodes.[119] Unfortunately, the study of the formation of the SEI and related passivation layers is limited by the fact that they are commonly very thin (between 5 and a few tens of nm) and consist of compounds containing functional groups similar to those present in the electrolyte they originate from, which is present inside the cell.

Despite that fact, coupling synchrotron radiation with FTIR microspectroscopy (SR-μFTIR) has great potential to study

operando battery materials, as the synchrotron infrared source is 100–1000 times brighter than a conventional thermal (*e.g.* Globar) sources.[120] Moreover, its high brightness (*i.e.* flux density) allows smaller regions (3–10 μm) to be probed in microscopy using different operation modes like transmission or reflection, suitable for *operando* battery analysis with an acceptable signal-to-noise ratio.[121]

In addition to the brightness advantage, the synchrotron source has other unique features. For example, the broad band of the synchrotron light enables FTIR spectroscopy to exploit the full infrared spectrum expanding from the far- to near-infrared regions of the electromagnetic spectrum. This is essential for determining the physical properties of solid-state components, to study surface science, as well as for the characterization of the chemical composition.[122]

Other advantages over the conventional thermal sources are a pulsed time structure and a high degree of polarization, which facilitate the combination of different techniques in a multimodal approach, especially when varying photon energies or frequencies are required. In this context, combining X-ray scattering, X-ray fluorescence (XRF) and X-ray absorption (XAS) with infrared microspectroscopic analysis on the same sample is of interest for a wide range of the materials research community. For instance, synchrotron infrared nanospectroscopy (SINS) combining synchrotron IR spectroscopy with scattering scanning near-field optical microscopy (s-SNOM) enables ultrabroadband infrared spectroscopy with nanometer spatial resolution beyond the Abbe limit (25 nm spatial resolution)[123] and was used to investigate, *in situ*, the chemical composition of non-aqueous metal–air electrodes.[124] For the sake of comparison, SR-μFTIR, with tens of micrometers field of view, allows a larger scale analysis area, while SINS enables estimating the chemical homogeneity at the nanodomain scale.

Despite the above-mentioned advantages, to the best of our knowledge there is currently no report on *operando* battery μFTIR measurement using synchrotron radiation. This can be rationalized considering the significant challenges associated with the development of a suitable electrochemical cell. Indeed, *in situ*/*operando* experiments using the attenuated total reflectance ATR-FTIR technique require the presence of an IR crystal of high refractive index (*i.e.* Ge, ZnSe, and diamond) and an IR transparent window (Fig. 8). The latter should be thin enough to allow for the required frequency range of the incident light to reach the sample and be reflected back to the detector. In addition to that, the presence of a thin layer of the electrolyte in the optical pathway can also represent a great challenge in terms of data treatment as the signal related to the electrolyte could mask the one originating from the system to be investigated.

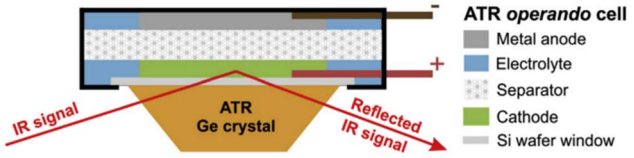

Fig. 8 Schematic representation of the ATR-IR pouch cell on a Ge ATR crystal. Reproduced from ref. 119.

Another important parameter to account for in ATR-FTIR measurement mode is the probing depth (d_p), typically ranging between a few hundreds of nm and 10–15 μm.[119]

$$d_p = \frac{\lambda}{2\pi\sqrt{n_1^2 \sin^2\theta - n_2^2}} \quad (2)$$

with (λ) the wavelength of the light, (θ) the angle of incidence, and (n_1) and (n_2) the refraction indices of the IR transparent window and the probed medium, respectively (Fig. 7). Therefore, a higher penetration depth can be achieved using a low refractive index transparent window and measuring in the low frequency region. However, most of the signal is associated with the small fraction of the electrode/electrolyte (<*ca.* 15 μm) portion in direct contact with the transparent window. In order to minimize the contribution from the bulk electrolyte, FTIR difference spectra can be obtained by subtracting the initial spectrum before the start of the electrochemical characterization from each of the obtained IR spectra during cell operation.[119]

Most *operando* IR battery measurements were performed using (ATR-FTIR) spectroscopy coupled to conventional thermal sources in the mid-IR spectral range where high (spatial and temporal) resolutions are not required for which SR should not provide significant improvement in terms of data quality or spectral resolution. Overall, the main advantage of SR over conventional in-house sources is thus expected to be mostly related to far-FTIR spectroscopy and FTIR microspectroscopy, which is yet a challenging approach.

Far-IR spectroscopy (terahertz region) is a robust tool to probe many of the fundamental spectral features of the inorganic materials used in batteries since they exhibit a considerable number of rotational modes and characteristic vibrations in the low-wavenumber region of the IR spectrum. Yet, synchrotron far-IR spectroscopy *operando* or *ex situ* studies on battery materials have not been reported to date.

Most of the reported ATR-FTIR *in situ*/*operando* studies on battery materials focus on single point measurements (around 100 μm of diameter) obtained through co-added scans FTIR spectra during cell operation. This approach can however be misguiding as it is complicated to know if the point sampled is representative of the entire electrode. Therefore, it is necessary to perform multiple/raster scan measurements to verify the chemical composition along the electrodes and the data collected can be used to visualize chemical differences across the sample.[125] Each pixel in a FTIR image is a complete infrared spectrum and hence by generating a sequence of FTIR images, it is conceivable to track variations in both space and time. Since the IR intensity of conventional sources is normally weak at high spatial resolutions (3–10 μm), especially when used in reflection (surface characterization), it requires a relatively long time (several minutes) to produce spectra with an acceptable signal-to-noise ratio at each measurement point and raster scanning experiments can be quite time consuming. The use of

synchrotron-based FTIR imaging is thus a very promising alternative allowing hundreds of measurements to be rapidly performed over a large area of the electrodes with improved spatial resolution and serves as well to detect heterogeneities.

Imaging techniques

Most spectroscopic techniques offer the possibility to implement space resolution by recording a position-dependent signal that can be used to map the sample. This is even more true with synchrotron techniques where the beam can be typically focused in a micrometric-sized spot, thus accessing a scale which can be relevant for materials in the battery field. As partially mentioned in the other sections, it is possible to map samples with XRD,[39,40] XPS,[115] X-ray fluorescence (XRF)[126] or infrared, usually with resolution in the micrometer range. In this section, the most widespread techniques will be discussed, mostly related to the classical radiography, which bases its contrast on the variable absorption of a physical object in the space. These X-ray imaging techniques allow for the visualization of battery materials and components by accessing morphological and structural information down to the nanometer scale. X-ray radiography is indeed widely used in batteries to non-destructively investigate failure in commercial cylindrical and pouch cells. Deviations from the regular cell layer geometry, such as those caused by gas evolution, are readily visualized and therefore X-ray systems have become a conventional method for industrial battery inspection and quality control. If the images can be taken at several different orientations of the sample relative to the X-ray beam, it is possible to reconstruct the 3D structure *via* specific tomographic algorithms. The use of synchrotron radiation not only allows *operando* experiments to be performed as a result of decreasing radiographic 3D acquisition time, but can also greatly improve contrast on equal acquisition times, which for instance help in the visualization of the electrolyte. Also, by tuning energy it is possible to combine imaging with spectroscopy, enabling chemical characterization with spatial resolution and therefore draw correlations between the sample morphology and composition.

A classification of synchrotron imaging techniques

Advanced imaging methods using synchrotron radiation are often classified into two broad groups: real space (lens-limited) and lens-less methods. To the first group belong full field Transmission X-ray Microscopy (abbreviated simply as TXM) and Scanning Transmission X-ray Microscopy (STXM); the second includes projection microscopy and coherent scattering techniques, mainly ptychography. These four experimental setups are depicted in Fig. 9a–d.

As schematized in Fig. 9a and b, for full-field and scanning modes the spatial resolution is limited by the lens numerical aperture (NA), *i.e.* the angular acceptance of the lens, to several X-ray wavelengths. In both cases, a spatial resolution down to 10 nm was demonstrated.[128,129] In TXM (Fig. 9a), the sample is placed in the middle of two lenses, the condenser lens before

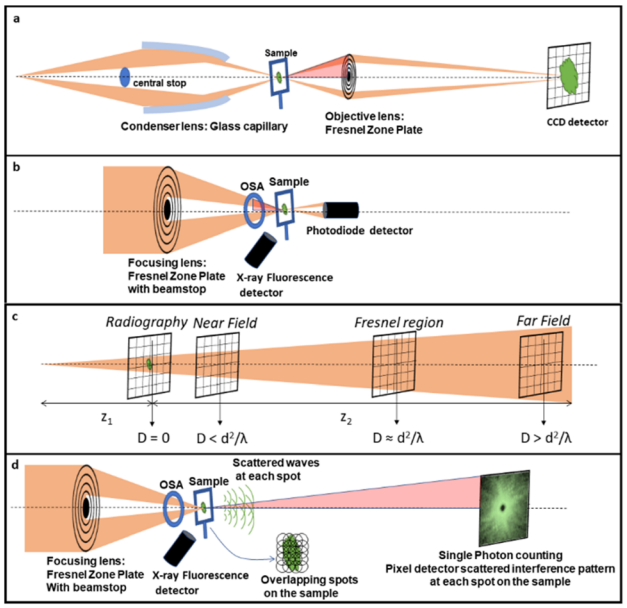

Fig. 9 Schematic representation of the four discussed techniques.[127] (a) TXM, (b) STXM, (c) projection microscopy and (d) ptychography. In (a), (b) and (d) the numerical aperture (NA), *i.e.* the maximum angle at which the imaging system is able to collect photons from the sample is reported as a light red angle. The bigger is the NA, the larger will be the maximum collectable spatial frequency, and the smaller will be the spatial resolution in the image. In (c) the different imaging regimes in projection microscopy are given as a function of the 'defocusing distance' $D = z1 \times z2/(z1 + z2)$. Distances are not to scale.

the sample and the objective lens after the sample. The objective is the one that practically limits not only the spatial resolution but also the depth of focus of the imaging system.[130,131] TXM is also compatible with Zernicke-type X-ray phase contrast.[132] Phase contrast effects are intensity modulations due to the interference of beams caused by phase shifts that are induced by the interaction with a heterogeneous sample. In general, phase contrast techniques are particularly valuable when absorption is weak, as in the case of hard X-rays interaction with low absorbing (low Z) elements. In a STXM (Fig. 9b), a lens is placed before the sample, providing a well-focalized beam at the sample plane. The sample is then raster-scanned in the focalized beam, and the spot size will define the lateral resolution of the system.[130,131] TXM is typically better in terms of the data acquisition speed with respect to STXM, which facilitates dynamic *operando* studies. The STXM setup is compatible with the acquisition of different types of signals (*e.g.*, transmission, fluorescence, diffraction, TEY, *etc.*) which can be recorded simultaneously at each sample position. Among them, fluorescence detection results in elemental and chemical analysis with the best sensitivity and it is therefore often used as a complementary technique to simultaneous STXM.[133] Another advantage of STXM is that since there are no lenses placed after the sample all the photons that reach it contribute to the image formation. This minimizes the necessary total dose delivered to the sample to achieve an acceptable signal-to-noise ratio and contrast, but not the resulting dose per unit time, which has to

be always taken into account in the STXM scheme to consider possible beam damage of the sample.[134] In projection microscopy (Fig. 9c), the image of the sample on the detector is obtained without the use of any lens, with the simplest experimental setup often also scaled down from the synchrotron to laboratory sources. In the particular case in which the detector is placed just after the sample, the setup is identical to standard radiography and the spatial resolution is directly determined by the detector pixel size. If instead the distance between the sample and the detector is large enough, the beam divergence can produce some magnification, and more importantly, also phase contrast effects.[127] Among all the possible lens-less phase contrast techniques, the direct propagation-based phase contrast is the simplest experimental setup.[135] The corresponding spatial resolution will depend on the used geometry[136] and typically spans from several microns down to the sub-microns scale. For intermediate propagation distances ('Fresnel region' regime in Fig. 9c), the technique is usually called holography,[137] whereas if the propagation distance is big enough ('far field' regime in Fig. 9c), widening the detected area well beyond the cone of beam illumination enables the so called 'coherent scattering imaging'.[135] In both cases, information on the sample structure and morphology can be deduced from the intensity distribution recorded on the detector *via* a 'phase retrieval' numerical reconstruction algorithm. Ptychography is the most frequent implementation of the coherent scattering- or diffraction-based imaging methods. In this case (see Fig. 8d), the object is illuminated by a coherent X-ray beam much smaller than the object size to image and the corresponding scattering pattern is recorded. Either the illumination or the sample is then shifted to a position with some overlap with the previous spot and the diffraction pattern recorded again. This process is repeated until the area of interest has been completely scanned. Because of the redundancy of information due to overlapping, phase retrieval algorithms converge quickly on a robust solution for both the object and the incident X-ray field. In this case, it is the detector geometry which limits the NA of the system, allowing for spatial resolutions down to a few nm (ref. 138) at the cost of the acquisition time. Interestingly, the ptychography setup is similar to the one used for STXM and both techniques may be implemented on the same instrument.[139] The four techniques summarized in Fig. 9 can be used with either hard or soft X-rays and all allow tomographic 3D reconstructions if the cell can be rotated in an angular range big enough to collect enough information.[140] When spatial resolutions below 100 nm are obtained in 3D by tomography, it is usual to refer to it as nano-tomography or, when it is implemented with the phase contrast approach, as phase-contrast nano-tomography.

Hard *vs.* soft X-rays

As mentioned before, the main factor determining the design of the experimental setups for *operando* experiments is the radiation penetration depth. In addition, for hard X-rays tomographic reconstruction in projection modality, the ideal cell allows the full sample inside the detector field of view (typically of the order of millimetres) without shadowing the sample at any angle, in such a way to have a full image of the system for full 180° rotation. In this sense, the best design is probably a cylindrical cell.[141] For a typical hard X-ray experiment, a regular electrode in a coin cell can be measured without the need for vacuum and hence the vast majority of the experiments reported in the literature use hard X-rays. In the presence of Fresnel Zone Plate (ZP) lenses typically used in TXM objectives and STXMs, the focal length is proportional to the energy and hence much bigger lens-to-sample distances are possible for hard X-rays when compared to soft X-rays, to the point that for high spatial resolution ZPs (<15 nm), the distance to the sample is not practically viable. Also, the small penetration depth in the soft X-ray energy region requires miniaturization of the cell, which is not compatible with a cylindrical cell geometry increasing the technical difficulty. Despite these disadvantages, the strong absorption of soft X-rays induces a lower detection threshold, which enables access to chemical composition even in individual active particles. As already mentioned in the spectroscopy section, soft X-rays also allow accessing specific absorption edges, such as the K edges of Li, B, C, N, O and F (practically the only option to directly probe the chemical environment of these elements) and the L and M edges for several transition metals which can provide complementary information to the K lines, as they are much more sensitive to the oxidation states.[142]

Hard X-ray tomography and spectro-microscopy

In the first *operando* synchrotron TXM study on a battery in 2010, the microstructural changes of Sn particles used as negative electrodes for Li-ion batteries were investigated. During electrochemical alloying with lithium, expansion and crack formation were revealed while recrystallization and partial contraction upon dealloying were observed particularly affecting the largest particles.[143] The first chemical mapping at <30 nm resolution was shown by energy dependent 2D images across the Cu K-edge on CuO particles,[144] which although not of conventional use in batteries also show the typical conversion mechanism found in several negative electrodes. These reactions typically introduce large disorder in the material and XAS is most suited to investigate local changes. The microscopy study revealed the evolution of the material even after stopping current and faster volume changes occurring in smaller particles, confirming a particle size-dependent mechanism. Remarkably, in addition to the morphology, the bulk composition of particles of up to 10 μm allows localizing with precision the electrochemically active regions and their response to external bias, with reduction starting from the surface of particles.

Operando 3D tomography was first exploited with a cell that could be rotated 180°, on rather large SnO particles (10–30 μm) with a 2 μm resolution.[145] In this case, an entire electrode, 16 mm diameter and 50 μm thick, was sampled, and typical crack evolution at the particle level was identified. In addition, different lithiation degrees in different electrode regions were inferred from the attenuation coefficient of absorption. First

a Sn + Li_2O composite was detected which was followed by an increase in Li-rich Li–Sn alloys, which are progressively less radiation absorbing because of the increased Li content. Absorption microtomography has become quite well established for *operando* studies in batteries, particularly for electrode materials containing heavy elements such as Sn and Ge, which provide the best contrast. Phase-contrast techniques are instead preferable for electrodes based on lighter elements. A 3D representation is particularly valuable in systems where the inherent reaction is a deposition process, such as the case of Li/S batteries, where degradation mechanisms can be sensitive to the morphological evolution of the deposits. The combination of absorption and phase contrast can be useful to discriminate different phases as shown in Fig. 10b. The sulfur particles, initially encapsulated by the binder to retain polysulfides, are progressively found distributed in the carbon electrode, while empty binder shells are left (Fig. 10d), which shows the failure of the encapsulation approach to prevent polysulfide dissolution.[146] 3D tomographic studies for this same battery technology have also revealed the coarsening of S particles in real carbon electrodes and depletion close to the separator[147] resolving binder domains and electrolyte-filled bulk pores.[141]

Si electrodes have been widely studied by phase-contrast tomography. Particle cracking, electrode volume, porosity evolution, and gas formation in the pores can be now quantified with a voxel size of 50 nm.[148] These studies have been also combined with SXRD in the thickness of an electrode to track the presence of $Li_{15}Si_4$, which induces undesired volume expansion and strains/cracks in the electrode.[149] Attempts have involved even metal-air batteries, where alkali oxides are particularly lightweight and with low absorption contrast with respect to carbon electrodes.[150]

Several *operando* studies have been reported for flow batteries, exploiting the difference in contrast between air and the electrolyte. The flow battery performance critically depends on the actual electrochemically active surface area and the electrolyte wetting of the carbon felt electrodes. Synchrotron X-ray tomography allowed the study of the effect of electrode compression on the electrolyte wetting of porous carbon electrodes.[151] The flow distribution inside electrodes of different geometry was instead inferred by studying the flooding mechanism of the cell by the electrolyte at different flow speeds.[152]

These few examples illustrate that standard microtomography is useful to detect phenomena such as particle fragmentation or detachment enabling comprehensive sample statistics of geometric parameters. However, the picture may not be complete if resolution is not submicrometric, as the mechanical properties of smaller particles may significantly deviate from those of larger ones. Techniques able to attain nm resolution such as X-ray phase contrast nano-tomography seem a better compromise for submicrometric scale studies enabling statistics over several thousands of particle aggregates of a few μm, which can be considered representative of commercial battery electrodes. The detail of information makes possible sophisticated and precise parametrization of the particle geometry and arrangement, so that the particle architecture and electrode mesostructure can be optimized for electrochemical performance in a better way than with standard microtomography.[153] However, in practice *operando* nanotomography has revealed quite challenging,[153] mainly because of the small sampled volume, often below 50 μm in size, in comparison to the several hundred micrometers or mm typical for microtomography. This requires extremely precise cell assembly and alignment of the electrodes with cuts delimiting the studied region. However, their position can still be easily affected by expansion/contraction phenomena taking place during cell operation. Besides, even if employing high energy radiation that is weakly absorbed and generally considered non-invasive, the high intensity of the focused beam can cause interactions in the form of heating, binder disconnections, bubbles, and deviations from identical electrodes measured *ex situ*.[150]

Taking tomography images at different energies across an absorption edge *in situ* (*i.e.* pausing the electrical current during measurements) is considered to produce a so-called "5D" data set. Through a marker-less tomographic technique that simplifies sample preparation and automatizes alignment, 5D acquisition has been demonstrated by Wang *et al.*[154] on a $LiFePO_4$ electrode (Fig. 11) using a cell fitted inside a quartz capillary, to allow complete rotation. Characterization relied on a full-field hard X-ray TXM at the Fe K-edge deconvoluting spectra as combinations of $LiFePO_4$ and $FePO_4$ references with results indicating a biphasic mechanism with the absence of intermediate phases. Remarkably, this was only unambiguously inferred from 3D images, as 2D projection maps showed artefacts that might have been misinterpreted as intermediate phases present.

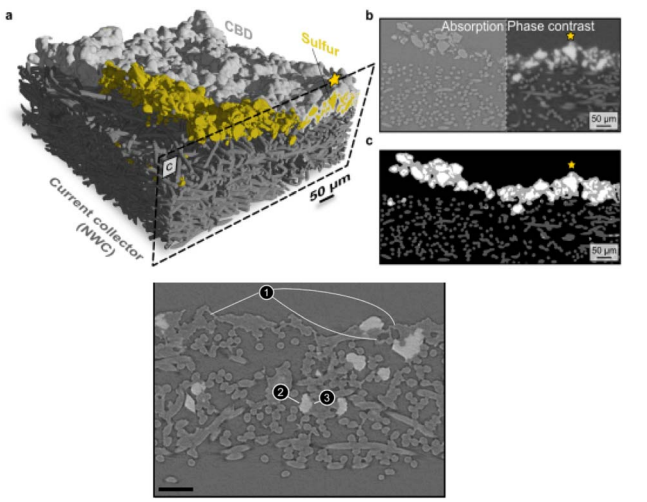

Fig. 10 (a) 3D reconstruction of a pristine sulfur electrode showing non-woven carbon paper (NWC, dark grey) and Carbon-Binder Domains (CBD, light grey) coating the sulfur particles (yellow), with CBD partially removed to show sulfur; (b) comparison of absorption and phase contrast slices from the 3D segmentation; (c) combination of absorption and phase contrast segmentation (colours as in (a), except for sulfur, here in white). The star marks the same particle in the three images; (d) absorption X-ray image of the electrode after 2 cycles showing empty CBD shells (1) and white sulfur particles. In contact with the pore space (2) or with the conducting network (3). Reproduced from ref. 146.

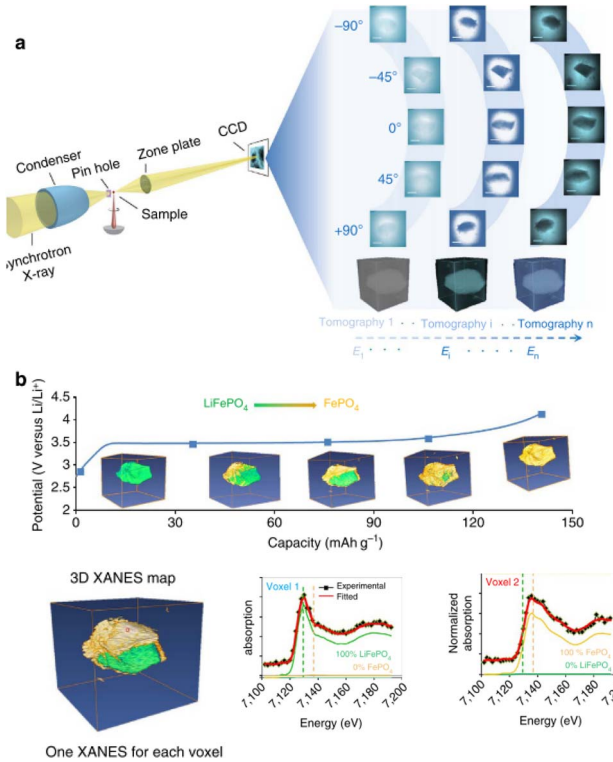

Fig. 11 Illustration of a 5D Fe K-edge XANES tomography. (a) Schematic of the experimental setup. A tomography data set is collected at different energies across the near Fe K-edge absorption to access chemical information for each voxel. By fitting the resulting spectra as a linear combination of spectra of end-phases, phase composition can be assigned to each voxel (right side). (b) Chemical phase distribution as a function of capacity (proportional to time). Reproduced from ref. 154.

Soft X-ray tomography and spectro-microscopy

Because of their small penetration depth, the experimental requirements for soft X-rays are similar to those needed when electrons are detected. This makes the technical developments for TEM in the past decade also useful with soft X-rays: open cells (using ionic liquids, Li_2O-coated Li or other solid state electrolytes), sealed miniaturized liquid cells,[155] and solid state cells.

Miniaturized liquid cells allowing *operando* TEM have been developed in the past decade.[156] Also several commercial systems are available, and their use with soft X-rays has been proposed (see for instance ref. 157). Typical cells adapted for soft X-rays *operando* imaging with liquid electrolytes consist of a flat transparent region, from a few hundreds of nanometres to ≈1 μm in thickness, confined between two ultrathin silicon nitride windows (typically <100 nm) and coupled with a microfluidic system with potential biasing[158,159] (see Fig. 12 for a scheme). In the case of STXM in fluorescence mode, transmission is not required and hence the cell geometry can be simplified, with just one transparent window, and no submicrometric sample thickness.[160] The construction of these miniaturized cells is in general significantly more challenging and expensive than the cells used in hard X-ray microscopy.

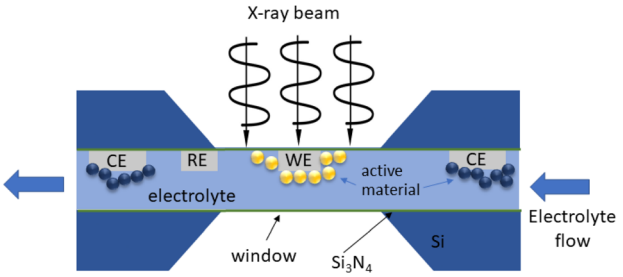

Fig. 12 Schematics of an electrochemical cell for *operando* TEM. The electrodes (WE: working; RE: reference; CE: counter) are connected to an external potentiostat.

Their representativity with respect to commercial batteries is hence limited and must be considered as setups for model experiments. Indeed, the thicknesses of the electrodes and electrolyte are so reduced that even the electrochemical processes may be affected. Although finite element calculations have shown that at the typical extremely low currents used the concentration and potential gradients in the electrolyte are negligible,[158] the presence of flow and turbulences, the discrete deposited particles, and their contact with the current collector may all affect these miniaturized cells to a larger extent than macroscopic ones. There is certainly a need for understanding the details of the electrochemistry on such configurations, which might also be relevant for microbatteries. Also the radiochemistry of the irradiation at different soft X-ray energies on the most typical battery chemistries need an assessment. Indeed, a rich radical chemistry has been shown for electron irradiation on organic electrolytes of interest for lithium batteries.[161] Complex radical cascades are induced by solvated electrons, involving solvent molecules and particularly salt anions. As a result, beam-induced electrochemistry can be observed, even in the absence of cell bias, sometimes preventing a reliable *operando* observation of electrode processes. For this reason, commercial TEM *operando* goniometers offer flow options for the electrolyte in a liquid cell, so that at least *in situ* observation can be interleaved with electrochemical operation, washing away the products of irradiation before electrochemistry is resumed. With X-ray radiation, although also significantly ionizing, a comparatively less dramatic radiolysis is expected, but this needs systematic assessment.

In spite of these constraints, some remarkable results have been achieved also with soft X-ray microscopy. The high spatial resolution was exploited in a detailed soft X-ray STXM study on 30 $LiFePO_4$ particles of realistic size. It demonstrated slow and fast domains, and a different evolution upon oxidation and reduction.[158] The biphasic behaviour was found to turn to a solid solution at a high rate with heterogeneities increasing/decreasing during delithiation and relithiation respectively. The observation of these phenomena provided key details in the understanding of the redox mechanism of this material, widely used in commercial batteries. Interestingly, a follow up study by soft X-ray ptychography[157] enabled insights into the particle morphology (Fig. 13A–C) and chemical speciation thanks to the better spatial resolution (≈7 nm, still 4.3× the X-ray wavelength

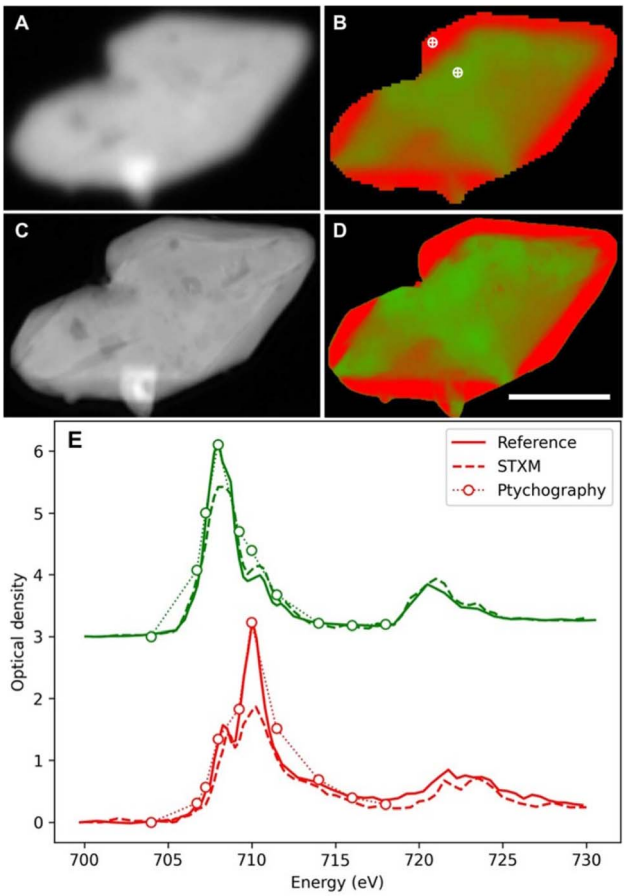

Fig. 13 Comparison between conventional STXM (A and B) and ptychographic (C and D) spectromicroscopy images of Li_xFePO_4 microplatelets. The average optical density (A and C) and the chemical composition map (B and D) where the two chemical components ($LiFePO_4$ and $FePO_4$) are presented in green and red, respectively (scale bar is 1 μm; reconstructed pixel size 5 nm). (E) Point spectra from the dots marked in (B) by conventional STXM (dashed lines) and ptychographic modes (dotted lines with circles). Reference spectra from pure materials ($LiFePO_4$, green solid line; $FePO_4$, red solid line) are also shown for comparison. The conventional STXM spectra show distortions that flatten the sharpest peaks, corresponding to energies where the difference in absorption between phases is maximum. The different attenuation overweighs the more abundant phase and instead the ptychographic spectra more closely match the pure references. Reproduced from ref. 157.

but 7× better than the STXM approach). Although qualitative agreement between the obtained chemical maps (Fig. 13D and E) is evident, the ptychographic one depicts nanoscale chemical phase features inside the particles, which are not visible with conventional STXM.

As a result of the cell setups being more straightforward when using solid electrolytes, the 3D morphological and chemical evolution of solid state batteries using X-ray tomography *operando* is quite established. Electrochemically driven phase changes, formation of cracks, contact loss and formation of interphases that increase electrode–electrolyte interface resistances have been visualized. For instance, the void formation at the interface between lithium and the $Li_{10}SnP_2S_{12}$ solid electrolyte was identified by X-ray tomography as the primary cell failure cause.[162] The chemomechanical interactions between the FeS_2 conversion electrode material and a $Li_7P_3S_{11}$ solid electrolyte were also studied by *operando* synchrotron X-ray nanotomography, which in this case enabled the detection of the loss of contact and build-up of metallic Fe which penalized Li diffusion, mitigated with a specially designed 3D electrode microstructure.[163]

Discussion and outlook

Battery research in general and in particular understanding the phenomena taking place not only at the electrodes but also at interfaces and interphases requires characterization techniques across multiple length scales which enable deconvolution of bulk and surface processes.[2] This is relevant for both mature technologies (such as Li-ion) for which the current focus is on optimizing the figures of merit in terms of not only electrochemical performance but also cycle life, and also for the development of new technologies. As shown in the different sections, *in situ* or *operando* synchrotron X-ray techniques have played a key role in the continuous progress in battery science, thanks to their capability to provide accurate information on the oxidation state of the redox active element, local and average structure, and morphological information under relevant conditions. *Operando* characterization is indeed crucial for the understanding of redox mechanisms and dynamic processes, and thus synchrotron based techniques are especially valuable due to their high temporal and spatial resolution. The possibility of changing photon energy brings about intrinsic advantages while at the same time adding complexity to the picture: soft X-rays, which are more surface and light-element sensitive, require a high vacuum and hence experimental setups less representative of realistic systems.

All the above-mentioned techniques probe complementary aspects, while at the same time presenting different technical advantages and disadvantages, which have resulted in different maturity levels. To access which phases are composing the electrode materials and how they are evolving as a function of cycling, XRD, PDF and XAS are exploited. They probe the averaged and local structures with XRD accessing only crystalline phases and PDF and EXAFS needing a well-defined model for quantification, where different correlated parameters can bias interpretation. Microscopy may instead provide this information more immediately in a qualitative way but at a local scale, while FTIR and soft X-ray XAS provide precious information on the organic compounds at either the electrodes, electrolytes or interphases, which are typically not accessible by XRD, hard X-ray XAS, or PDF. XAS and XES can be exploited to assess charge compensation mechanisms being naturally complementary as they probe unoccupied and occupied electronic levels, respectively. Yet, since the spectral features depend on the electronic properties, site symmetry, and nature of bonding with surrounding ligands, their interpretation is not straightforward unless different edges are probed and/or different techniques are coupled.

One of the crucial aspects to assess is the improvement of cell design to be able to carry out *operando* experiments in setups which are representative of real battery operation.

Indeed, while real pouch or even stainless steel casing coin or cylindrical cells can be used under very specific conditions, customized cells are the norm. Even if practical parameters such as the electrode formulation or the electrode/electrolyte amount ratio mimic realistic systems as much as possible, geometrical constrains may induce changes in the electric field lines which can have an influence on the electrochemical performance and hence also some impact on the phenomena investigated. As mentioned above, the complexity of the processes taking place during battery operation calls for the development of multi-modal characterization, *i.e.* the use of more than one technique in the same experiment (not necessarily both being synchrotron based), is a clear path to follow which enable achieving a more holistic understanding of the mechanisms involved. Ideally, it should involve the use of the same optimized cell setup and either correlative or even simultaneous standardized workflows, minimizing beam-induced effects, while at the same time adjusting the spectral response to the required time scale to follow cell dynamics. The development of an "ideal" cell representative of real batteries and suitable for any multimodal approach does not seem realistic, especially considering that the portfolio of techniques used is rapidly expanding, each of them coming with their own technical/geometrical requirements. However, as mentioned in the section devoted to electrochemical cells and setup requirements, progress in cell design has been outstanding in recent years, with some designs available (some being commercialized) that can already be used for a wide variety of techniques.

All *operando* synchrotron experiments are expected to allow non-invasive and non-destructive probing of materials under real conditions and hence enable even the detection of metastable intermediate species. However, ensuring that the beam has no effect on the investigated material is challenging. On one hand, exposure to high energy radiation can induce beam-induced effects and control experiments are mandatory to assess the reliability of data interpretation. If the beam induces some sort of irreversible damage (*e.g.* on the binder/carbon matrix),[164] they will be more easily identified. Yet, effects can be more subtle and disappear when irradiation is stopped, which can make its detection more difficult, especially if new battery chemistries are investigated[165] for which no standard components exist. These aspects become specially challenging for XAS and in particular for proper EXAFS measurements, as these require in general a relatively long exposition time at energies where intense absorption is present. Interaction with the beam is complex and can involve the emission of photoelectrons, Auger electron cascades, radiolysis phenomena, radical formation, electrolyte decomposition and gas bubble generation.[5,165] Therefore, acquisition conditions need to be carefully optimized in each experiment to minimize beam induced effects. Typical strategies[166] consist in defocusing the beam, reducing the local exposure time, performing stroboscopic measurements where acquisition is alternated with rest times, average measurements at different positions and attenuating the beam intensity. It will be critical to study and control all these phenomena in view of the ongoing shift to 4th generation synchrotron sources and free-electron lasers, which offer orders of magnitude higher photon intensities. These may open the possibility to greatly reduce exposure times but radiation damage induced by dose rate may still be a limiting factor. For such reasons we expect that when spectromicroscopy and tomography are used in the same experiment, it will remain practically unlikely to achieve true *operando* conditions due to the actual exposure times required. It will rather be preferable to stop the reaction and deal with *in situ* experiments, which generally do not imply the loss of reliability. For instance, comparable conclusions were drawn from *ex situ* soft X-ray TXM measurements[167] and TEM *operando*[168] studies on Na/O_2 batteries, which can be considered a mutual validation for both techniques on this specific system. Overall, as in other research fields, common sense and a judicious choice of the methodology should prevail to make the most efficient use of available resources while maximizing scientific progress.

Another overriding and growing concern related to *operando* characterization is the huge amount of data produced, and the difficulties of their subsequent analysis. Different automated data treatment protocols have been recently developed such as the Pearson correlation coefficient, enabling to detect subtle changes in the materials present during high-throughput *operando* diffraction experiments,[169,170] while also allowing to take decisions during data collection thanks to its mathematical simplicity. Other more mathematically complex methods, such as non-negative matrix factorization, have been developed to assist in elucidating the phases present/appearing in microscopy images or *operando* series.[171,172] However, automated analysis able to obtain more physical information is only starting, *e.g.* following the profile changes of specific graphite diffraction peaks to infer the succession of stages formed during the redox process.[173] The need to perform Rietveld refinements on a large number of successive XRD patterns has been addressed developing specific software enabling either automated fitting of single diffractograms (that can be expanded in a relatively simple way)[174] or more complete tools specifically designed for sequential refinement of *operando* patterns.[175] The complexity and instrument specificity of the data harvested using other techniques (and even also diffraction) clearly call for further developments in this area, with progress in big data and artificial intelligence being a clear asset. Besides data analysis, the automation of multi-technique data acquisition using standardized workflows would bring in a paradigm shift in *operando* characterization, especially if standardized cells could also be designed.[3]

Given the recent evolution achieved in these areas, accelerated progress is expected in the years to come which will certainly improve our ability to understand battery mechanisms at an atomic level and hence develop new chemistries while at the same time getting the most out of the already commercialized concepts.

Author contributions

All authors contributed to writing and revision of the manuscript.

Conflicts of interest

There are no conflicts to declare.

Acknowledgements

The authors are grateful for funding through PTI+ TRANSENER+: "Alta Tecnología clave en la transición en el ciclo energético", part of the CSIC program for the Spanish Recovery, Transformation and Resilience Plan funded by the Recovery and Resilience Facility of the European Union, established by the Regulation (EU) 2020/2094. ICMAB-CSIC members thank the Spanish Agencia Estatal de Investigación Severo Ochoa Programme for Centres of Excellence in R&D (CEX2019-000917-S).

Notes and references

1 M. R. Palacin, Battery Materials Design Essentials, *Acc. Mater. Res.*, 2021, **2**(5), 319–326, DOI: **10.1021/accountsmr.1c00026**.

2 D. Atkins, E. Ayerbe, A. Benayad, *et al.*, Understanding Battery Interfaces by Combined Characterization and Simulation Approaches: Challenges and Perspectives, *Adv. Energy Mater.*, 2022, **12**(17), 2102687, DOI: **10.1002/aenm.202102687**.

3 D. Atkins, E. Capria, K. Edström, *et al.*, Accelerating Battery Characterization Using Neutron and Synchrotron Techniques: Toward a Multi-Modal and Multi-Scale Standardized Experimental Workflow, *Adv. Energy Mater.*, 2022, **12**(17), 2102694, DOI: **10.1002/AENM.202102694**.

4 F. Lin, Y. Liu, X. Yu, *et al.*, Synchrotron X-ray Analytical Techniques for Studying Materials Electrochemistry in Rechargeable Batteries, *Chem. Rev.*, 2017, **117**(21), 13123–13186, DOI: **10.1021/acs.chemrev.7b00007**.

5 O. J. Borkiewicz, K. M. Wiaderek, P. J. Chupas and K. W. Chapman, Best Practices for Operando Battery Experiments: Influences of X-ray Experiment Design on Observed Electrochemical Reactivity, *J. Phys. Chem. Lett.*, 2015, **6**(11), 2081–2085, DOI: **10.1021/acs.jpclett.5b00891**.

6 M. P. B. Glazer, J. S. Okasinski, J. D. Almer and Y. Ren, High-energy x-ray scattering studies of battery materials, *MRS Bull.*, 2016, **41**(6), 460–465, DOI: **10.1557/MRS.2016.96/FIGURES/5**.

7 G. Liang, J. Hao, A. M. D'Angelo, V. K. Peterson, Z. Guo and W. K. Pang, A Robust Coin-Cell Design for In Situ Synchrotron-based X-Ray Powder Diffraction Analysis of Battery Materials, *Batteries Supercaps*, 2021, **4**(2), 380–384, DOI: **10.1002/BATT.202000218**.

8 K. Choudhary, I. O. Santos Mendoza, A. Nadeina, *et al.*, Operando X-ray diffraction in transmission geometry "at home" from tape casted electrodes to all-solid-state battery, *J. Power Sources*, 2023, **553**, 232270, DOI: **10.1016/J.JPOWSOUR.2022.232270**.

9 A. v. Llewellyn, A. Matruglio, D. J. L. Brett, R. Jervis and P. R. Shearing, Using In-Situ Laboratory and Synchrotron-Based X-ray Diffraction for Lithium-Ion Batteries Characterization: A Review on Recent Developments, *Condens. Matter*, 2020, **5**(4), 75, DOI: **10.3390/CONDMAT5040075**.

10 D. Saurel, A. Pendashteh, M. Jáuregui, *et al.*, Experimental Considerations for Operando Metal-Ion Battery Monitoring using X-ray Techniques, *Chem.: Methods*, 2021, **1**(6), 249–260, DOI: **10.1002/CMTD.202100009**.

11 O. Gustafsson, A. Schökel and W. R. Brant, Design and Operation of an Operando Synchrotron Diffraction Cell Enabling Fast Cycling of Battery Materials, *Batteries Supercaps*, 2021, **4**(10), 1599–1604, DOI: **10.1002/BATT.202100126**.

12 C. Xu, K. Märker, J. Lee, *et al.*, Bulk fatigue induced by surface reconstruction in layered Ni-rich cathodes for Li-ion batteries, *Nat. Mater.*, 2020, **20**(1), 84–92, DOI: **10.1038/s41563-020-0767-8**.

13 O. J. Borkiewicz, B. Shyam, K. M. Wiaderek, C. Kurtz, P. J. Chupas and K. W. Chapman, The AMPIX electrochemical cell: a versatile apparatus for in situ X-ray scattering and spectroscopic measurements, *J. Appl. Crystallogr.*, 2012, **45**(6), 1261–1269, DOI: **10.1107/S0021889812042720**.

14 O. A. Drozhzhin, I. V. Tereshchenko, H. Emerich, E. V. Antipov, A. M. Abakumov and D. Chernyshov, An electrochemical cell with sapphire windows for operando synchrotron X-ray powder diffraction and spectroscopy studies of high-power and high-voltage electrodes for metal-ion batteries, *J. Synchrotron Radiat.*, 2018, **25**(2), 468–472, DOI: **10.1107/S1600577517017489**.

15 J. Sottmann, R. Homs-Regojo, D. S. Wragg, H. Fjellvåg, S. Margadonna and H. Emerich, Versatile electrochemical cell for Li/Na-ion batteries and high-throughput setup for combined operando X-ray diffraction and absorption spectroscopy, *J. Appl. Crystallogr.*, 2016, **49**(6), 1972–1981, DOI: **10.1107/S160057671601428X/RG5119SUP1.PDF**.

16 C. Villevieille, T. Sasaki and P. Novák, Novel electrochemical cell designed for operando techniques and impedance studies, *RSC Adv.*, 2014, **4**(13), 6782–6789, DOI: **10.1039/C3RA46184J**.

17 M. Herklotz, J. Weiß, E. Ahrens, *et al.*, A novel high-throughput setup for in situ powder diffraction on coin cell batteries, *J. Appl. Crystallogr.*, 2016, **49**(1), 340–345, DOI: **10.1107/S1600576715022165/KC5016SUP1.PDF**.

18 R. G. Houdeville, A. P. Black, A. Ponrouch, M. R. Palacín and F. Fauth, Operando Synchrotron X-ray Diffraction Studies on TiS2: The Effect of Propylene Carbonate on Reduction Mechanism, *J. Electrochem. Soc.*, 2021, **168**(3), 030514, DOI: **10.1149/1945-7111/ABE983**.

19 C. Wu, Y. Lei, L. Simonelli, *et al.*, Continuous Carbon Channels Enable Full Na-Ion Accessibility for Superior Room-Temperature Na–S Batteries, *Adv. Mater.*, 2022, **34**(8), 2108363, DOI: **10.1002/ADMA.202108363**.

20 F. Strauss, D. Kitsche, Y. Ma, *et al.*, Operando Characterization Techniques for All-Solid-State Lithium-Ion Batteries, *Adv. Energy Sustain. Res.*, 2021, **2**(6), 2100004, DOI: **10.1002/AESR.202100004**.

21 R. G. Houdeville, Synchrotron powder diffraction on operando batteries at non-ambient temperature, TDX

(Tesis Doctorals en Xarxa), Published online October 7, 2021, Accessed August 1, 2022, https://www.tdx.cat/handle/10803/674417.

22 J. B. Leriche, S. Hamelet, J. Shu, *et al.*, An Electrochemical Cell for Operando Study of Lithium Batteries Using Synchrotron Radiation, *J. Electrochem. Soc.*, 2010, **157**(5), A606, DOI: 10.1149/1.3355977/XML.

23 T. Broux, F. Fauth, N. Hall, *et al.*, High Rate Performance for Carbon-Coated Na3V2(PO4)2F3 in Na-Ion Batteries, *Small Methods*, 2019, **3**(4), 1800215, DOI: 10.1002/SMTD.201800215.

24 T. Taskovic, A. Eldesoky, W. Song, M. Bauer and J. R. Dahn, High Temperature Testing of NMC/Graphite Cells for Rapid Cell Performance Screening and Studies of Electrolyte Degradation, *J. Electrochem. Soc.*, 2022, **169**(4), 040538, DOI: 10.1149/1945-7111/AC6453.

25 M. V. Blanco, D. Devaux, A. M. Valtavirta, *et al.*, Simultaneous Monitoring of Structural Changes and Phase Distribution of LiFePO4 Along the Cathode Thickness of Li Metal Polymer Battery, *J. Electrochem. Soc.*, 2020, **167**(16), 160517, DOI: 10.1149/1945-7111/ABCD4D.

26 H. Fujimoto, S. Takagi, K. Shimoda, *et al.*, Analysis of Intercalation/De-Intercalation of Li Ions Into/From Graphite at 0 °C via Operando Synchrotron X-ray Diffraction, *J. Electrochem. Soc.*, 2021, **168**(9), 090515, DOI: 10.1149/1945-7111/AC2280.

27 C. J. Pan, C. Yuan, G. Zhu, *et al.*, An operando X-ray diffraction study of chloroaluminate anion-graphite intercalation in aluminum batteries, *Proc. Natl. Acad. Sci. U. S. A.*, 2018, **115**(22), 5670–5675, DOI: 10.1073/PNAS.1803576115/SUPPL_FILE/PNAS.1803576115.SAPP.PDF.

28 R. R. Chianelli, J. C. Scanlon and B. M. L. Rao, Dynamic X-Ray Diffraction, *J. Electrochem. Soc.*, 1978, **125**(10), 1563–1566, DOI: 10.1149/1.2131244.

29 M. Bianchini, F. Fauth, E. Suard, J. B. Leriche, C. Masquelier and L. Croguennec, Spinel materials for Li-ion batteries: new insights obtained by operando neutron and synchrotron X-ray diffraction, *Acta Crystallogr., Sect. B: Struct. Sci., Cryst. Eng. Mater.*, 2015, **71**(6), 688–701, DOI: 10.1107/S2052520615017199.

30 S. Park, Z. Wang, Z. Deng, *et al.*, Crystal Structure of Na2V2(PO4)3, an Intriguing Phase Spotted in the Na3V2(PO4)3–Na1V2(PO4)3 System, *Chem. Mater.*, 2022, **34**(1), 451–462, DOI: 10.1021/acs.chemmater.1c04033.

31 A. P. Black, D. Monti, C. Frontera, *et al.*, Operando Synchrotron X-ray Diffraction in Calcium Batteries: Insights into the Redox Activity of 1D Ca3CoMO6 (M = Co and Mn), *Energy Fuels*, 2021, **35**(13), 10898–10907, DOI: 10.1021/acs.energyfuels.1c01343.

32 X. Zhang, M. van Hulzen, D. P. Singh, *et al.*, Rate-Induced Solubility and Suppression of the First-Order Phase Transition in Olivine LiFePO4, *Nano Lett.*, 2014, **14**(5), 2279–2285, DOI: 10.1021/nl404285y.

33 M. Bianchini, F. Fauth, N. Brisset, *et al.*, Comprehensive Investigation of the Na3V2(PO4)2F3–NaV2(PO4)2F3 System by Operando High Resolution Synchrotron X-ray Diffraction, *Chem. Mater.*, 2015, **27**(8), 3009–3020, DOI: 10.1021/acs.chemmater.5b00361.

34 C. D. Quilty, P. J. West, G. P. Wheeler, *et al.*, Elucidating Cathode Degradation Mechanisms in $LiNi_{0.8}Mn_{0.1}Co_{0.1}O_2$ (NMC811)/Graphite Cells Under Fast Charge Rates Using Operando Synchrotron Characterization, *J. Electrochem. Soc.*, 2022, **169**(2), 020545, DOI: 10.1149/1945-7111/ac51f5.

35 X. Zhang, M. van Hulzen, D. P. Singh, *et al.*, Direct view on the phase evolution in individual LiFePO4 nanoparticles during Li-ion battery cycling, *Nat. Commun.*, 2015, **6**(1), 8333, DOI: 10.1038/ncomms9333.

36 S. Tardif, N. Dufour, J. F. Colin, *et al.*, Combining operando X-ray experiments and modelling to understand the heterogeneous lithiation of graphite electrodes, *J. Mater. Chem. A*, 2021, **9**(7), 4281–4290, DOI: 10.1039/D0TA10735B.

37 L. Romano Brandt, J. J. Marie, T. Moxham, *et al.*, Synchrotron X-ray quantitative evaluation of transient deformation and damage phenomena in a single nickel-rich cathode particle, *Energy Environ. Sci.*, 2020, **13**(10), 3556–3566, DOI: 10.1039/D0EE02290J.

38 H. Liu, Z. Li, A. Grenier, *et al.*, Best practices for operando depth-resolving battery experiments, *J. Appl. Crystallogr.*, 2020, **53**(1), 133–139, DOI: 10.1107/S1600576719016315.

39 A. C. Marschilok, A. M. Bruck, A. Abraham, *et al.*, Energy dispersive X-ray diffraction (EDXRD) for operando materials characterization within batteries, *Phys. Chem. Chem. Phys.*, 2020, **22**(37), 20972–20989, DOI: 10.1039/D0CP00778A.

40 K. P. C. Yao, J. S. Okasinski, K. Kalaga, I. A. Shkrob and D. P. Abraham, Quantifying lithium concentration gradients in the graphite electrode of Li-ion cells using operando energy dispersive X-ray diffraction, *Energy Environ. Sci.*, 2019, **12**(2), 656–665, DOI: 10.1039/C8EE02373E.

41 F. Sun, K. Dong, M. Osenberg, *et al.*, Visualizing the morphological and compositional evolution of the interface of InLi-anode|thio-LISION electrolyte in an all-solid-state Li–S cell by in operando synchrotron X-ray tomography and energy dispersive diffraction, *J. Mater. Chem. A*, 2018, **6**(45), 22489–22496, DOI: 10.1039/C8TA08821G.

42 G. A. Elia, G. Greco, P. H. Kamm, F. García-Moreno, S. Raoux and R. Hahn, Simultaneous X-Ray Diffraction and Tomography Operando Investigation of Aluminum/Graphite Batteries, *Adv. Funct. Mater.*, 2020, **30**(43), 2003913, DOI: 10.1002/adfm.202003913.

43 H. Charalambous, D. P. Abraham, A. R. Dunlop, *et al.*, Revealing causes of macroscale heterogeneity in lithium ion pouch cells via synchrotron X-ray diffraction, *J. Power Sources*, 2021, **507**, 230253, DOI: 10.1016/j.jpowsour.2021.230253.

44 X. Yu, Z. Feng, Y. Ren, *et al.*, Simultaneous Operando Measurements of the Local Temperature, State of Charge, and Strain inside a Commercial Lithium-Ion Battery Pouch Cell, *J. Electrochem. Soc.*, 2018, **165**(7), A1578–A1585, DOI: 10.1149/2.1251807jes.

45 H. He, B. Liu, A. Abouimrane, *et al.*, Dynamic Lithium Intercalation/Deintercalation in 18650 Lithium Ion Battery by Time-Resolved High Energy Synchrotron X-Ray Diffraction, *J. Electrochem. Soc.*, 2015, **162**(10), A2195–A2200, DOI: 10.1149/2.0771510jes.

46 M. R. Cosby, G. M. Carignan, Z. Li, *et al.*, Operando Synchrotron Studies of Inhomogeneity during Anode-Free Plating of Li Metal in Pouch Cell Batteries, *J. Electrochem. Soc.*, 2022, **169**(2), 020571, DOI: 10.1149/1945-7111/ac5345.

47 S. J. L. Billinge, The rise of the X-ray atomic pair distribution function method: a series of fortunate events, *Philos. Trans. R. Soc., A*, 2019, **377**(2147), 20180413, DOI: 10.1098/RSTA.2018.0413.

48 M. Diaz-Lopez, G. L. Cutts, P. K. Allan, *et al.*, Fast operando X-ray pair distribution function using the DRIX electrochemical cell, *J. Synchrotron Radiat.*, 2020, **27**(5), 1190–1199, DOI: 10.1107/S160057752000747X.

49 J. Sottmann, M. di Michiel, H. Fjellvåg, *et al.*, Chemical Structures of Specific Sodium Ion Battery Components Determined by Operando Pair Distribution Function and X-ray Diffraction Computed Tomography, *Angew. Chem., Int. Ed.*, 2017, **56**(38), 11385–11389, DOI: 10.1002/ANIE.201704271.

50 J. M. Stratford, A. K. Kleppe, D. S. Keeble, *et al.*, Correlating Local Structure and Sodium Storage in Hard Carbon Anodes: Insights from Pair Distribution Function Analysis and Solid-State NMR, *J. Am. Chem. Soc.*, 2021, **143**(35), 14274–14286, DOI: 10.1021/JACS.1C06058/ASSET/IMAGES/LARGE/JA1C06058_0007.JPEG.

51 D. Saurel, J. Segalini, M. Jauregui, *et al.*, A SAXS outlook on disordered carbonaceous materials for electrochemical energy storage, *Energy Storage Mater.*, 2019, **21**, 162–173, DOI: 10.1016/J.ENSM.2019.05.007.

52 C. L. Berhaut, D. Z. Dominguez, P. Kumar, *et al.*, Multiscale Multiphase Lithiation and Delithiation Mechanisms in a Composite Electrode Unraveled by Simultaneous Operando Small-Angle and Wide-Angle X-Ray Scattering, *ACS Nano*, 2019, **13**(10), 11538–11551, DOI: 10.1021/ACSNANO.9B05055/ASSET/IMAGES/MEDIUM/NN9B05055_M002.GIF.

53 C. L. Berhaut, D. Z. Dominguez, D. Tomasi, *et al.*, Prelithiation of silicon/graphite composite anodes: Benefits and mechanisms for long-lasting Li-Ion batteries, *Energy Storage Mater.*, 2020, **29**, 190–197, DOI: 10.1016/J.ENSM.2020.04.008.

54 C. Prehal, A. Samojlov, M. Nachtnebel, *et al.*, In situ small-angle X-ray scattering reveals solution phase discharge of Li-O2 batteries with weakly solvating electrolytes, *Proc. Natl. Acad. Sci. U. S. A.*, 2021, **118**(14), e2021893118, DOI: 10.1073/PNAS.2021893118/SUPPL_FILE/PNAS.2021893118.SAPP.PDF.

55 J. McBreen, The application of synchrotron techniques to the study of lithium-ion batteries, *J. Solid State Electrochem.*, 2009, **13**(7), 1051–1061, DOI: 10.1007/S10008-008-0685-1/FIGURES/9.

56 A. Mottana and A. Marcelli, The Historical Development of X-ray Absorption Fine Spectroscopy and of Its Applications to Materials Science, *History of Mechanism and Machine Science*, 2015, vol. 27, pp. 275–301, DOI: 10.1007/978-94-017-9645-3_15/COVER.

57 S. E. Ali, W. Olszewski, C. Marini, *et al.*, Quantification of charge compensation in lithium- and manganese-rich Li-ion cathode materials by x-ray spectroscopies, *Mater. Today Phys.*, 2022, **24**, 100687, DOI: 10.1016/J.MTPHYS.2022.100687.

58 Y. Yu, P. Karayaylali, D. Sokaras, *et al.*, Towards controlling the reversibility of anionic redox in transition metal oxides for high-energy Li-ion positive electrodes, *Energy Environ. Sci.*, 2021, **14**(4), 2322–2334, DOI: 10.1039/D0EE03765F.

59 W. Olszewski, M. Ávila Pérez, C. Marini, *et al.*, Temperature Dependent Local Structure of NaxCoO2 Cathode Material for Rechargeable Sodium-Ion Batteries, *J. Phys. Chem. C*, 2016, **120**(8), 4227–4232, DOI: 10.1021/ACS.JPCC.5B10885/ASSET/IMAGES/JP-2015-10885R_M002.GIF.

60 G. Aquilanti, M. Giorgetti, R. Dominko, *et al.*, Operando characterization of batteries using x-ray absorption spectroscopy: advances at the beamline XAFS at synchrotron Elettra, *J. Phys. D: Appl. Phys.*, 2017, **50**(7), 074001, DOI: 10.1088/1361-6463/AA519A.

61 J. Timoshenko and B. Roldan Cuenya, In Situ/Operando Electrocatalyst Characterization by X-ray Absorption Spectroscopy, *Chem. Rev.*, 2021, **121**(2), 882–961, DOI: 10.1021/ACS.CHEMREV.0C00396/ASSET/IMAGES/LARGE/CR0C00396_0027.JPEG.

62 L. Mino, G. Agostini, P. Ghigna and E. Quartarone, Operando x-ray absorption spectroscopy on battery materials: a review of recent developments, *J. Phys.: Energy*, 2021, **3**(3), 032006, DOI: 10.1088/2515-7655/ABF2DB.

63 C. Lévy-Clément, C. Mondoloni, C. Godart and R. Cortès, In Situ X-Ray Diffraction and In Situ X-Ray Absorption Spectroscopy for Investigation of Intercalation Batteries: Application to the Alkaline H+/γ-MnO2 system, *MRS Online Proc. Libr.*, 1990, **210**(1), 387–398, DOI: 10.1557/PROC-210-387.

64 X. Q. Yang, K. H. Xue, H. S. Lee, J. McBreen, T. A. Skotheim and F. Lu, X-ray-absorption studies of organodisulfide redox polymeric electrodes, *Phys. Rev. B*, 1992, **45**(10), 5733, DOI: 10.1103/PhysRevB.45.5733.

65 X. Wang, H. Zhou, Z. Chen and X. Meng, Synchrotron-based X-ray diffraction and absorption spectroscopy studies on layered LiNixMnyCozO2 cathode materials: A review, *Energy Storage Mater.*, 2022, **49**, 181–208, DOI: 10.1016/J.ENSM.2022.04.012.

66 K. Luo, M. R. Roberts, R. Hao, *et al.*, Charge-compensation in 3d-transition-metal-oxide intercalation cathodes through the generation of localized electron holes on oxygen, *Nat. Chem.*, 2016, **8**(7), 684–691, DOI: 10.1038/nchem.2471.

67 G. Assat, A. Iadecola, C. Delacourt, R. Dedryvère and J. M. Tarascon, Decoupling Cationic-Anionic Redox Processes in a Model Li-Rich Cathode via Operando X-ray Absorption Spectroscopy, *Chem. Mater.*, 2017, **29**(22),

9714–9724, DOI: 10.1021/ACS.CHEMMATER.7B03434/ASSET/IMAGES/LARGE/CM-2017-03434E_0006.JPEG.

68 W. S. Yoon, C. P. Grey, M. Balasubramanian, X. Q. Yang, D. A. Fischer and J. McBreen, Combined NMR and XAS Study on Local Environments and Electronic Structures of Electrochemically Li-Ion Deintercalated Li1-xCo 1/3Ni1/3Mn1/3O2 Electrode System, *Electrochem. Solid-State Lett.*, 2004, **7**(3), A53, DOI: 10.1149/1.1643592/XML.

69 M. Balasubramanian, J. McBreen, I. J. Davidson, P. S. Whitfield and I. Kargina, In Situ X-Ray Absorption Study of a Layered Manganese-Chromium Oxide-Based Cathode Material, *J. Electrochem. Soc.*, 2002, **149**(2), A176, DOI: 10.1149/1.1431962/XML.

70 J. R. Croy, M. Balasubramanian, D. Kim, S. H. Kang and M. M. Thackeray, Designing high-capacity, lithium-ion cathodes using x-ray absorption spectroscopy, *Chem. Mater.*, 2011, **23**(24), 5415–5424, DOI: 10.1021/CM2026703/ASSET/IMAGES/LARGE/CM-2011-026703_0008.JPEG.

71 L. Simonin, J. F. Colin, V. Ranieri, *et al.*, In situ investigations of a Li-rich Mn–Ni layered oxide for Li-ion batteries, *J. Mater. Chem.*, 2012, **22**(22), 11316–11322, DOI: 10.1039/C2JM31205K.

72 M. A. Lowe, J. Gao and H. D. Abruña, In operando X-ray studies of the conversion reaction in Mn3O4 lithium battery anodes, *J. Mater. Chem. A*, 2013, **1**(6), 2094–2103, DOI: 10.1039/C2TA01270G.

73 W. Olszewski, I. Isturiz, C. Marini, *et al.*, Effects of nanostructuring on the bond strength and disorder in V2O5 cathode material for rechargeable ion-batteries, *Phys. Chem. Chem. Phys.*, 2018, **20**(22), 15288–15292, DOI: 10.1039/C8CP00716K.

74 M. Fehse, A. Iadecola, L. Simonelli, A. Longo and L. Stievano, The rise of X-ray spectroscopies for unveiling the functional mechanisms in batteries, *Phys. Chem. Chem. Phys.*, 2021, **23**(41), 23445–23465, DOI: 10.1039/D1CP03263A.

75 Y. N. Zhou, J. L. Yue, E. Hu, *et al.*, High-Rate Charging Induced Intermediate Phases and Structural Changes of Layer-Structured Cathode for Lithium-Ion Batteries, *Adv. Energy Mater.*, 2016, **6**(21), 1600597, DOI: 10.1002/AENM.201600597.

76 X. F. Luo, J. Patra, W. T. Chuang, *et al.*, Charge–Discharge Mechanism of High-Entropy Co-Free Spinel Oxide Toward Li+ Storage Examined Using Operando Quick-Scanning X-Ray Absorption Spectroscopy, *Adv. Sci.*, 2022, **9**(21), 2201219, DOI: 10.1002/ADVS.202201219.

77 V. Briois, C. la Fontaine, S. Belin, *et al.*, ROCK: the new Quick-EXAFS beamline at SOLEIL, *J. Phys.: Conf. Ser.*, 2016, **712**(1), 012149, DOI: 10.1088/1742-6596/712/1/012149.

78 J. Stötzel, D. Lützenkirchen-Hecht and R. Frahm, A new flexible monochromator setup for quick scanning x-ray absorption spectroscopy, *Rev. Sci. Instrum.*, 2010, **81**(7), 073109, DOI: 10.1063/1.3458015.

79 O. Müller, D. Lützenkirchen-Hecht and R. Frahm, Quick scanning monochromator for millisecond in situ and in operando X-ray absorption spectroscopy, *Rev. Sci. Instrum.*, 2015, **86**(9), 093905, DOI: 10.1063/1.4929866.

80 F. Yang, X. Feng, Y. S. Liu, *et al.*, In Situ/Operando (Soft) X-ray Spectroscopy Study of Beyond Lithium-ion Batteries, *Energy Environ. Mater.*, 2021, **4**(2), 139–157, DOI: 10.1002/EEM2.12172.

81 X. Liu, D. Wang, G. Liu, *et al.*, Distinct charge dynamics in battery electrodes revealed by in situ and operando soft X-ray spectroscopy, *Nat. Commun.*, 2013, **4**(1), 1–8, DOI: 10.1038/ncomms3568.

82 M. Schellenberger, R. Golnak, W. G. Quevedo Garzon, S. Risse and R. Seidel, Accessing the solid electrolyte interphase on silicon anodes for lithium-ion batteries in-situ through transmission soft X-ray absorption spectroscopy, *Mater. Today Adv.*, 2022, **14**, 100215, DOI: 10.1016/J.MTADV.2022.100215.

83 J. J. Velasco-Velez, C. H. Wu, T. A. Pascal, *et al.*, Interfacial water. The structure of interfacial water on gold electrodes studied by x-ray absorption spectroscopy, *Science*, 2014, **346**(6211), 831–834, DOI: 10.1126/SCIENCE.1259437.

84 Y. Ye, C. H. Wu, L. Zhang, Y. S. Liu, P. A. Glans-Suzuki and J. Guo, Using soft x-ray absorption spectroscopy to characterize electrode/electrolyte interfaces in-situ and operando, *J. Electron Spectrosc. Relat. Phenom.*, 2017, **221**, 2–9, DOI: 10.1016/J.ELSPEC.2017.05.002.

85 M. Cuisinier, P. E. Cabelguen, S. Evers, *et al.*, Sulfur speciation in Li-S batteries determined by operando X-ray absorption spectroscopy, *J. Phys. Chem. Lett.*, 2013, **4**(19), 3227–3232, DOI: 10.1021/JZ401763D/SUPPL_FILE/JZ401763D_SI_001.PDF.

86 Y. Yan, C. Cheng, L. Zhang, *et al.*, Deciphering the Reaction Mechanism of Lithium–Sulfur Batteries by In Situ/Operando Synchrotron-Based Characterization Techniques, *Adv. Energy Mater.*, 2019, **9**(18), 1900148, DOI: 10.1002/AENM.201900148.

87 Y. Gorlin, M. U. M. Patel, A. Freiberg, *et al.*, Understanding the Charging Mechanism of Lithium-Sulfur Batteries Using Spatially Resolved Operando X-Ray Absorption Spectroscopy, *J. Electrochem. Soc.*, 2016, **163**(6), A930–A939, DOI: 10.1149/2.0631606JES/XML.

88 E. Zhao, J. Wang, F. Li, *et al.*, Exploring reaction dynamics in lithium–sulfur batteries by time-resolved operando sulfur K-edge X-ray absorption spectroscopy, *Chem. Commun.*, 2019, **55**(34), 4993–4996, DOI: 10.1039/C9CC00485H.

89 K. Nakanishi, D. Kato, H. Arai, *et al.*, Novel spectro-electrochemical cell for in situ/operando observation of common composite electrode with liquid electrolyte by X-ray absorption spectroscopy in the tender X-ray region, *Rev. Sci. Instrum.*, 2014, **85**(8), 084103, DOI: 10.1063/1.4891036.

90 L. Simonelli, A. Sorrentino, C. Marini, *et al.*, Role of Manganese in Lithium- and Manganese-Rich Layered Oxides Cathodes, *J. Phys. Chem. Lett.*, 2019, 3359–3368, DOI: 10.1021/ACS.JPCLETT.9B01174/ASSET.

91 Z. W. Lebens-Higgins, H. Chung, M. J. Zuba, *et al.*, How Bulk Sensitive is Hard X-ray Photoelectron Spectroscopy: Accounting for the Cathode-Electrolyte Interface when Addressing Oxygen Redox, *J. Phys. Chem. Lett.*, 2020, **11**(6), 2106–2112, DOI: 10.1021/ACS.JPCLETT.0C00229/ASSET/IMAGES/LARGE/JZ0C00229_0004.JPEG.

92 T. C. Taucher, I. Hehn, O. T. Hofmann, M. Zharnikov and E. Zojer, Understanding Chemical versus Electrostatic Shifts in X-ray Photoelectron Spectra of Organic Self-Assembled Monolayers, *J. Phys. Chem. C*, 2016, **120**(6), 3428–3437, DOI: 10.1021/ACS.JPCC.5B12387/ASSET/IMAGES/LARGE/JP-2015-12387J_0007.JPEG.

93 X. Wu, C. Villevieille, P. Novák and M. el Kazzi, Monitoring the chemical and electronic properties of electrolyte–electrode interfaces in all-solid-state batteries using operando X-ray photoelectron spectroscopy, *Phys. Chem. Chem. Phys.*, 2018, **20**(16), 11123–11129, DOI: 10.1039/C8CP01213J.

94 M. P. Seah, An accurate and simple universal curve for the energy-dependent electron inelastic mean free path, *Surf. Interface Anal.*, 2012, **44**(4), 497–503, DOI: 10.1002/SIA.4816.

95 C. J. Powell, Practical guide for inelastic mean free paths, effective attenuation lengths, mean escape depths, and information depths in x-ray photoelectron spectroscopy, *J. Vac. Sci. Technol., A*, 2020, **38**(2), 023209, DOI: 10.1116/1.5141079.

96 S. Wi, V. Shutthanandan, B. M. Sivakumar, *et al.*, In situ x-ray photoelectron spectroscopy analysis of electrochemical interfaces in battery: Recent advances and remaining challenges, *J. Vac. Sci. Technol., A*, 2022, **40**(1), 010808, DOI: 10.1116/6.0001460.

97 R. Hausbrand, G. Cherkashinin, H. Ehrenberg, *et al.*, Fundamental degradation mechanisms of layered oxide Li-ion battery cathode materials: Methodology, insights and novel approaches, *Mater. Sci. Eng., B*, 2015, **192**(C), 3–25, DOI: 10.1016/J.MSEB.2014.11.014.

98 J. Maibach, C. Xu, S. K. Eriksson, *et al.*, A high pressure x-ray photoelectron spectroscopy experimental method for characterization of solid-liquid interfaces demonstrated with a Li-ion battery system, *Rev. Sci. Instrum.*, 2015, **86**(4), 044101, DOI: 10.1063/1.4916209.

99 S. Jacke, J. Song, G. Cherkashinin, L. Dimesso and W. Jaegermann, Investigation of the solid-state electrolyte/cathode LiPON/LiCoO2 interface by photoelectron spectroscopy, *Ionics*, 2010, **16**(9), 769–775, DOI: 10.1007/S11581-010-0479-1/FIGURES/8.

100 K. N. Wood, K. X. Steirer, S. E. Hafner, *et al.*, Operando X-ray photoelectron spectroscopy of solid electrolyte interphase formation and evolution in Li2S-P2S5 solid-state electrolytes, *Nat. Commun.*, 2018, **9**(1), 1–10, DOI: 10.1038/s41467-018-04762-z.

101 D. Tonti, C. Pettenkofer and W. Jaegermann, In-situ photoelectron spectroscopy study of a TiS2 thin film cathode in an operating Na intercalation electrochemical cell, *Ionics*, 2000, **6**(3), 196–202, DOI: 10.1007/BF02374066.

102 D. M. Itkis, D. A. Semenenko, E. Y. Kataev, *et al.*, Reactivity of carbon in lithium-oxygen battery positive electrodes, *Nano Lett.*, 2013, **13**(10), 4697–4701, DOI: 10.1021/NL4021649/SUPPL_FILE/NL4021649_SI_001.PDF.

103 X. Wu, M. Mirolo, C. A. F. Vaz, P. Novák and M. el Kazzi, Reactivity and Potential Profile across the Electrochemical LiCoO2-Li3PS4Interface Probed byOperandoX-ray Photoelectron Spectroscopy, *ACS Appl. Mater. Interfaces*, 2021, **13**(36), 42670–42681, DOI: 10.1021/ACSAMI.1C09605/SUPPL_FILE/AM1C09605_SI_001.PDF.

104 X. Wu, C. Villevieille, P. Novák and M. el Kazzi, Insights into the chemical and electronic interface evolution of Li4Ti5O12 cycled in Li2S–P2S5 enabled by operando X-ray photoelectron spectroscopy, *J. Mater. Chem. A*, 2020, **8**(10), 5138–5146, DOI: 10.1039/C9TA14147B.

105 M. Mirolo, X. Wu, C. A. F. Vaz, P. Novák and M. el Kazzi, Unveiling the Complex Redox Reactions of SnO2in Li-Ion Batteries Using Operando X-ray Photoelectron Spectroscopy and in Situ X-ray Absorption Spectroscopy, *ACS Appl. Mater. Interfaces*, 2021, **13**(2), 2547–2557, DOI: 10.1021/ACSAMI.0C17936/SUPPL_FILE/AM0C17936_SI_001.PDF.

106 H. Kiuchi, K. Hikima, K. Shimizu, R. Kanno, F. Toshiharu and E. Matsubara, Operando hard X-ray photoelectron spectroscopy of LiCoO2 thin film in an all-solid-state lithium ion battery, *Electrochem. Commun.*, 2020, **118**, 106790, DOI: 10.1016/J.ELECOM.2020.106790.

107 D. Weingarth, A. Foelske-Schmitz, A. Wokaun and R. Kötz, In situ electrochemical XPS study of the Pt/[EMIM][BF4] system, *Electrochem. Commun.*, 2011, **13**(6), 619–622, DOI: 10.1016/J.ELECOM.2011.03.027.

108 A. Kolmakov, D. A. Dikin, L. J. Cote, *et al.*, Graphene oxide windows for in situ environmental cell photoelectron spectroscopy, *Nat. Nanotechnol.*, 2011, **6**(10), 651–657, DOI: 10.1038/nnano.2011.130.

109 T. Masuda, H. Yoshikawa, H. Noguchi, *et al.*, In situ x-ray photoelectron spectroscopy for electrochemical reactions in ordinary solvents, *Appl. Phys. Lett.*, 2013, **103**(11), 111605, DOI: 10.1063/1.4821180.

110 J. J. Velasco-Velez, L. J. Falling, D. Bernsmeier, *et al.*, A comparative study of electrochemical cells for in situ x-ray spectroscopies in the soft and tender x-ray range, *J. Phys. D: Appl. Phys.*, 2021, **54**(12), 124003, DOI: 10.1088/1361-6463/ABD2ED.

111 S. Axnanda, E. J. Crumlin, B. Mao, *et al.*, Using "Tender" X-ray Ambient Pressure X-Ray Photoelectron Spectroscopy as A Direct Probe of Solid-Liquid Interface, *Sci. Rep.*, 2015, **5**(1), 1–12, DOI: 10.1038/srep09788.

112 S. Zhu, M. Scardamaglia, J. Kundsen, *et al.*, HIPPIE: a new platform for ambient-pressure X-ray photoelectron spectroscopy at the MAX IV Laboratory, *J. Synchrotron Radiat.*, 2021, **28**(2), 624–636, DOI: 10.1107/S160057752100103X.

113 J. Maibach, I. Källquist, M. Andersson, *et al.*, Probing a battery electrolyte drop with ambient pressure photoelectron spectroscopy, *Nat. Commun.*, 2019, **10**(1), 1–7, DOI: 10.1038/s41467-019-10803-y.

114 D. M. Itkis, J. J. Velasco-Velez, A. Knop-Gericke, A. Vyalikh, M. v. Avdeev and L. v. Yashina, Probing Operating

Electrochemical Interfaces by Photons and Neutrons, *ChemElectroChem*, 2015, **2**(10), 1427–1445, DOI: 10.1002/CELC.201500155.

115 K. Akada, T. Sudayama, D. Asakura, *et al.*, Microscopic photoelectron analysis of single crystalline LiCoO2 particles during the charge-discharge in an all solid-state lithium ion battery, *Sci. Rep.*, 2019, **9**(1), 1–7, DOI: 10.1038/s41598-019-48842-6.

116 M. Favaro, F. F. Abdi, E. J. Crumlin, Z. Liu, R. v. d. Krol and D. E. Starr, Interface Science Using Ambient Pressure Hard X-ray Photoelectron Spectroscopy, *Surfaces*, 2019, **2**(1), 78–99, DOI: 10.3390/SURFACES2010008.

117 K. D. Fulfer and D. G. Kuroda, Solvation Structure and Dynamics of the Lithium Ion in Organic Carbonate-Based Electrolytes: A Time-Dependent Infrared Spectroscopy Study, *J. Phys. Chem. C*, 2016, **120**(42), 24011–24022, DOI: 10.1021/ACS.JPCC.6B08607/ASSET/IMAGES/LARGE/JP-2016-08607X_0008.JPEG.

118 L. Meyer, D. Curran, R. Brow, S. Santhanagopalan and J. Porter, Operando Measurements of Electrolyte Li-ion Concentration during fast charging with FTIR/ATR, *J. Electrochem. Soc.*, 2021, **168**(9), 090502, DOI: 10.1149/1945-7111/AC1D7A.

119 J. Bitenc, A. Vizintin, J. Grdadolnik and R. Dominko, Tracking electrochemical reactions inside organic electrodes by operando IR spectroscopy, *Energy Storage Mater.*, 2019, **21**, 347–353, DOI: 10.1016/J.ENSM.2019.05.038.

120 G. P. Williams and W. D. Duncan, Infrared synchrotron radiation from electron storage rings, *Appl. Opt.*, 1983, **22**(18), 2914–2923, DOI: 10.1364/AO.22.002914.

121 J. A. Reffner, P. A. Martoglio and G. P. Williams, Fourier transform infrared microscopical analysis with synchrotron radiation: The microscope optics and system performance (invited), *Rev. Sci. Instrum.*, 1998, **66**(2), 1298, DOI: 10.1063/1.1145958.

122 C. N. Kotanen, F. Gabriel Moussy, S. Carrara and A. Guiseppi-Elie, Infrared Spectroscopy Using Synchrotron Radiation, *Encyclopedia of Biophysics*, 2013, pp. 1106–1112, DOI: 10.1007/978-3-642-16712-6_128.

123 H. A. Bechtel, E. A. Muller, R. L. Olmon, M. C. Martin and M. B. Raschke, Ultrabroadband infrared nanospectroscopic imaging, *Proc. Natl. Acad. Sci. U. S. A.*, 2014, **111**(20), 7191–7196, DOI: 10.1073/PNAS.1400502111/SUPPL_FILE/PNAS.201400502SI.PDF.

124 T. C. M. Nepel, C. G. Anchieta, L. F. Cremasco, *et al.*, In Situ Infrared Micro and Nanospectroscopy for Discharge Chemical Composition Investigation of Non-Aqueous Lithium–Air Cells, *Adv. Energy Mater.*, 2021, **11**(45), 2101884, DOI: 10.1002/AENM.202101884.

125 M. Tahtouh, J. R. Kalman, C. Roux, C. Lennard and B. J. Reedy, The Detection and Enhancement of Latent Fingermarks Using Infrared Chemical Imaging, *J. Forensic Sci.*, 2005, **50**(1), 64–72, Accessed August 1, 2022, https://www.astm.org.

126 C. Marini, A. M. D. Rovira, N. Ramanan, W. Olszewski, B. Joseph and L. Simonelli, Combined micro X-ray absorption and fluorescence spectroscopy to map phases of complex systems: the case of sphalerite, *Sci. Rep.*, 2019, **9**(1), 1–8, DOI: 10.1038/s41598-019-55347-9.

127 A. Pogany, D. Gao and S. W. Wilkins, Contrast and resolution in imaging with a microfocus x-ray source, *Rev. Sci. Instrum.*, 1998, **68**(7), 2774, DOI: 10.1063/1.1148194.

128 W. Chao, P. Fischer, T. Tyliszczak, *et al.*, Real space soft x-ray imaging at 10 nm spatial resolution, *Opt. Express*, 2012, **20**(9), 9777–9783, DOI: 10.1364/OE.20.009777.

129 H. Yan, N. Bouet, J. Zhou, *et al.*, Multimodal hard x-ray imaging with resolution approaching 10 nm for studies in material science, *Nano Futures*, 2018, **2**(1), 011001, DOI: 10.1088/2399-1984/AAB25D.

130 D. Attwood, Soft X-Rays and Extreme Ultraviolet Radiation: Principles and Applications, *Soft X-Rays and Extreme Ultraviolet Radiation*, 1999, DOI: 10.1017/CBO9781139164429.

131 M. Howells, C. Jacobsen, T. Warwick and A. van den Bos, Principles and Applications of Zone Plate X-Ray Microscopes, *Sci. Microsc.*, 2007, 835–926, DOI: 10.1007/978-0-387-49762-4_13.

132 Z. Su, V. de Andrade, S. Cretu, *et al.*, X-ray Nanocomputed Tomography in Zernike Phase Contrast for Studying 3D Morphology of Li-O2Battery Electrode, *ACS Appl. Energy Mater.*, 2020, **3**(5), 4093–4102, DOI: 10.1021/ACSAEM.9B02236/ASSET/IMAGES/LARGE/AE9B02236_0007.JPEG.

133 B. Bozzini, P. Bocchetta, G. Kourousias and A. Gianoncelli, Electrodeposition of Mn-Co/Polypyrrole Nanocomposites: An Electrochemical and In Situ Soft-X-ray Microspectroscopic Investigation, *Polymers*, 2017, **9**(1), 17, DOI: 10.3390/POLYM9010017.

134 M. Howellst and C. Jacobsen, Soft X-ray microscopes and their biological applications, *Q. Rev. Biophys.*, 1995, **28**(1), 33–130, DOI: 10.1017/S0033583500003139.

135 K. A. Nugent, Coherent methods in the X-ray sciences, *Adv. Phys.*, 2009, **59**(1), 1–99, DOI: 10.1080/00018730903270926.

136 A. Cedola, A. Sorrentino, A. M. Gerardino, *et al.*, X-ray phase contrast microscopy at 300 nm resolution with laboratory sources, *Opt. Express*, 2010, **18**(15), 15998–16004, DOI: 10.1364/OE.18.015998.

137 P. Cloetens, W. Ludwig, J. Baruchel, *et al.*, Holotomography: Quantitative phase tomography with micrometer resolution using hard synchrotron radiation x rays, *Appl. Phys. Lett.*, 1999, **75**(19), 2912, DOI: 10.1063/1.125225.

138 A. Diaz, P. Trtik, M. Guizar-Sicairos, A. Menzel, P. Thibault and O. Bunk, Quantitative x-ray phase nanotomography, *Phys. Rev. B: Condens. Matter Mater. Phys.*, 2012, **85**(2), 020104, DOI: 10.1103/PHYSREVB.85.020104/FIGURES/4/MEDIUM.

139 H. Yuan, H. Yuan, T. Casagrande, *et al.*, 4D Imaging of ZnO-Coated Nanoporous Al2O3Aerogels by Chemically Sensitive Ptychographic Tomography: Implications for Designer Catalysts, *ACS Appl. Nano Mater.*, 2021, **4**(1), 621–632, DOI: 10.1021/ACSANM.0C02924/SUPPL_FILE/AN0C02924_SI_004.MP4.

140 J. Liu, Y. Guan, L. Chen, *et al.*, Locating the "missing wedge" artifacts from limited-angle CT reconstruction, *Microsc. Microanal.*, 2018, **24**(S2), 138–139, DOI: 10.1017/S1431927618013089.

141 C. Tan, T. M. M. Heenan, R. F. Ziesche, *et al.*, Four-Dimensional Studies of Morphology Evolution in Lithium-Sulfur Batteries, *ACS Appl. Energy Mater.*, 2018, **1**(9), 5090–5100, DOI: 10.1021/ACSAEM.8B01148/SUPPL_FILE/AE8B01148_SI_002.AVI.

142 C. H. Lin, K. Sun, M. Ge, *et al.*, Systems-level investigation of aqueous batteries for understanding the benefit of water-in-salt electrolyte by synchrotron nanoimaging, *Sci. Adv.*, 2020, **6**(10), 7129–7135, DOI: 10.1126/SCIADV.AAY7129/SUPPL_FILE/AAY7129_SM.PDF.

143 S. C. Chao, Y. C. Yen, Y. F. Song, Y. M. Chen, H. C. Wu and N. L. Wu, A study on the interior microstructures of working Sn particle electrode of Li-ion batteries by in situ X-ray transmission microscopy, *Electrochem. Commun.*, 2010, **12**(2), 234–237, DOI: 10.1016/J.ELECOM.2009.12.002.

144 J. Wang, Y. C. K. Chen-Wiegarta and J. Wang, In situ chemical mapping of a lithium-ion battery using full-field hard X-ray spectroscopic imaging, *Chem. Commun.*, 2013, **49**(58), 6480–6482, DOI: 10.1039/C3CC42667J.

145 M. Ebner, F. Marone, M. Stampanoni and V. Wood, Visualization and quantification of electrochemical and mechanical degradation in Li ion batteries, *Science*, 2013, **342**(6159), 716–720, DOI: 10.1126/SCIENCE.1241882.

146 L. Zielke, C. Barchasz, S. Walu, *et al.*, Degradation of Li/S Battery Electrodes On 3D Current Collectors Studied Using X-ray Phase Contrast Tomography, *Sci. Rep.*, 2015, **5**(1), 1–12, DOI: 10.1038/srep10921.

147 A. Yermukhambetova, C. Tan, S. R. Daemi, *et al.*, Exploring 3D microstructural evolution in Li-Sulfur battery electrodes using in-situ X-ray tomography, *Sci. Rep.*, 2016, **6**(1), 1–9, DOI: 10.1038/srep35291.

148 V. Vanpeene, J. Villanova, J. P. Suuronen, *et al.*, Monitoring the morphological changes of Si-based electrodes by X-ray computed tomography: A 4D-multiscale approach, *Nano Energy*, 2020, **74**, 104848, DOI: 10.1016/J.NANOEN.2020.104848.

149 P. Pietsch, M. Hess, W. Ludwig, J. Eller and V. Wood, Combining operando synchrotron X-ray tomographic microscopy and scanning X-ray diffraction to study lithium ion batteries, *Sci. Rep.*, 2016, **6**(1), 1–10, DOI: 10.1038/srep27994.

150 Z. Su, T. T. Nguyen, C. l. Bourlot, *et al.*, Towards a Local In situ X-ray Nano Computed Tomography under Realistic Cycling Conditions for Battery Research, *Chem.: Methods*, 2022, **2**(5), e202100051, DOI: 10.1002/CMTD.202100051.

151 N. Bevilacqua, L. Eifert, R. Banerjee, *et al.*, Visualization of electrolyte flow in vanadium redox flow batteries using synchrotron X-ray radiography and tomography – Impact of electrolyte species and electrode compression, *J. Power Sources*, 2019, **439**, 227071, DOI: 10.1016/j.jpowsour.2019.227071.

152 K. Köble, L. Eifert, N. Bevilacqua, K. F. Fahy, A. Bazylak and R. Zeis, Synchrotron X-Ray radiography of vanadium redox flow batteries – Time and spatial resolved electrolyte flow in porous carbon electrodes, *J. Power Sources*, 2021, **492**, 229660, DOI: 10.1016/j.jpowsour.2021.229660.

153 J. Li, N. Sharma, Z. Jiang, *et al.*, Dynamics of particle network in composite battery cathodes, *Science*, 2022, **376**(6592), 517–521, DOI: 10.1126/SCIENCE.ABM8962/SUPPL_FILE/SCIENCE.ABM8962_SM.PDF.

154 J. Wang, Y. C. K. Chen-Wiegart, C. Eng, Q. Shen and J. Wang, Visualization of anisotropic-isotropic phase transformation dynamics in battery electrode particles, *Nat. Commun.*, 2016, **7**(1), 1–7, DOI: 10.1038/ncomms12372.

155 C. Han, M. T. Islam and C. Ni, In Situ TEM of Electrochemical Incidents: Effects of Biasing and Electron Beam on Electrochemistry, *ACS Omega*, 2021, **6**(10), 6537–6546, DOI: 10.1021/ACSOMEGA.0C05829.

156 J. Xie, J. Li, W. Mai and G. Hong, A decade of advanced rechargeable batteries development guided by in situ transmission electron microscopy, *Nano Energy*, 2021, **83**, 105780, DOI: 10.1016/J.NANOEN.2021.105780.

157 D. A. Shapiro, S. Babin, R. S. Celestre, *et al.*, An ultrahigh-resolution soft x-ray microscope for quantitative analysis of chemically heterogeneous nanomaterials, *Sci. Adv.*, 2020, **6**(51), eabc4904, DOI: 10.1126/sciadv.abc4904.

158 J. Lim, Y. Li, D. H. Alsem, *et al.*, Origin and hysteresis of lithium compositional spatiodynamics within battery primary particles, *Science*, 2016, **353**(6299), 566–571, DOI: 10.1126/SCIENCE.AAF4914/SUPPL_FILE/LIM.SM.PDF.

159 C. Gosse, S. Stanescu, J. Frederick, *et al.*, A pressure-actuated flow cell for soft X-ray spectromicroscopy in liquid media, *Lab Chip*, 2020, **20**(17), 3213–3229, DOI: 10.1039/C9LC01127G.

160 Y. Li, J. N. Weker, W. E. Gent, *et al.*, Dichotomy in the Lithiation Pathway of Ellipsoidal and Platelet LiFePO4 Particles Revealed through Nanoscale Operando State-of-Charge Imaging, *Adv. Funct. Mater.*, 2015, **25**(24), 3677–3687, DOI: 10.1002/ADFM.201500286.

161 P. Abellan, B. L. Mehdi, L. R. Parent, *et al.*, Probing the degradation mechanisms in electrolyte solutions for li-ion batteries by in situ transmission electron microscopy, *Nano Lett.*, 2014, **14**(3), 1293–1299, DOI: 10.1021/NL404271K/SUPPL_FILE/NL404271K_SI_008.AVI.

162 J. A. Lewis, F. J. Q. Cortes, Y. Liu, *et al.*, Linking void and interphase evolution to electrochemistry in solid-state batteries using operando X-ray tomography, *Nat. Mater.*, 2021, **20**(4), 503–510, DOI: 10.1038/s41563-020-00903-2.

163 N. Sun, Q. Liu, Y. Cao, *et al.*, Anisotropically Electrochemical–Mechanical Evolution in Solid-State Batteries and Interfacial Tailored Strategy, *Angew. Chem., Int. Ed.*, 2019, **58**(51), 18647–18653, DOI: 10.1002/ANIE.201910993.

164 C. Lim, H. Kang, V. de Andrade, F. de Carlo and L. Zhu, Hard X-ray-induced damage on carbon-binder matrix for in situ synchrotron transmission X-ray microscopy tomography of Li-ion batteries, *J. Synchrotron Radiat.*, 2017, **24**(3), 695–698, DOI: 10.1107/S1600577517003046/VV5162SUP6.PDF.

165 L. Blondeau, S. Surblé, E. Foy, H. Khodja, S. Belin and M. Gauthier, Are Operando Measurements of Rechargeable Batteries Always Reliable? An Example of Beam Effect with a Mg Battery, *Anal. Chem.*, 2022, **94**(27), 9683–9689, DOI: **10.1021/ACS.ANALCHEM.2C01056/SUPPL_FILE/AC2C01056_SI_001.PDF**.

166 X. Liu, D. Wang, G. Liu, *et al.*, Distinct charge dynamics in battery electrodes revealed by in situ and operando soft X-ray spectroscopy, *Nat. Commun.*, 2013, **4**(1), 1–8, DOI: **10.1038/ncomms3568**.

167 I. Landa-Medrano, A. Sorrentino, L. Stievano, *et al.*, Architecture of Na-O2 battery deposits revealed by transmission X-ray microscopy, *Nano Energy*, 2017, **37**, 224–231, DOI: **10.1016/J.NANOEN.2017.05.021**.

168 L. Lutz, W. Dachraoui, A. Demortière, *et al.*, Operando Monitoring of the Solution-Mediated Discharge and Charge Processes in a Na-O2 Battery Using Liquid-Electrochemical Transmission Electron Microscopy, *Nano Lett.*, 2018, **18**(2), 1280–1289, DOI: **10.1021/ACS.NANOLETT.7B04937/SUPPL_FILE/NL7B04937_SI_006.AVI**.

169 B. Aoun, C. Yu, L. Fan, Z. Chen, K. Amine and Y. Ren, A generalized method for high throughput in-situ experiment data analysis: An example of battery materials exploration, *J. Power Sources*, 2015, **279**, 246–251, DOI: **10.1016/J.JPOWSOUR.2015.01.033**.

170 T. A. Assefa, A. F. Suzana, L. Wu, *et al.*, Imaging the Phase Transformation in Single Particles of the Lithium Titanate Anode for Lithium-Ion Batteries, *ACS Appl. Energy Mater.*, 2021, **4**(1), 111–118, DOI: **10.1021/ACSAEM.0C02010/ASSET/IMAGES/LARGE/AE0C02010_0007.JPEG**.

171 H. Tanimoto, X. Hongkun, M. Mizumaki, *et al.*, Non-negative matrix factorization for 2D-XAS images of lithium ion batteries, *J. Phys. Commun.*, 2021, **5**(11), 115005, DOI: **10.1088/2399-6528/AC3268**.

172 P. M. Maffettone, A. C. Daly and D. Olds, Constrained non-negative matrix factorization enabling real-time insights of in situ and high-throughput experiments, *Appl. Phys. Rev.*, 2021, **8**(4), 041410, DOI: **10.1063/5.0052859**.

173 H. Fujimoto, H. Kiuchi, S. Takagi, *et al.*, Assessing Reaction Mechanisms of Graphite Negative Electrodes Based on Operando Synchrotron Radiation Diffraction Data, *J. Electrochem. Soc.*, 2021, **168**(4), 040509, DOI: **10.1149/1945-7111/ABF181**.

174 X. Cui, Z. Feng, Y. Jin, *et al.*, AutoFP: a GUI for highly automated Rietveld refinement using an expert system algorithm based on FullProf, *J. Appl. Crystallogr.*, 2015, **48**(5), 1581–1586, DOI: **10.1107/S1600576715015125**.

175 O. Arcelus, J. Rodriguez-Carvajal and N. Ayape Katcho, **https://github.com/oarcelus/FullProfAPP-beta**.